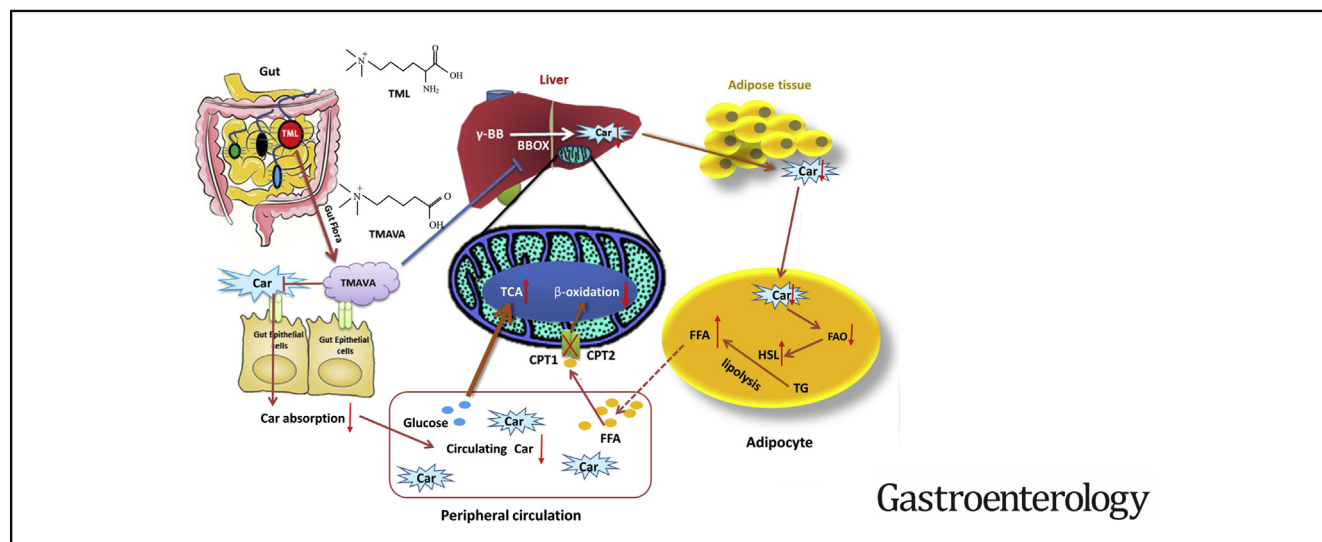




TMAVA, a Metabolite of Intestinal Microbes, Is Increased in Plasma From Patients With Liver Steatosis, Inhibits γ -Butyrobetaine Hydroxylase, and Exacerbates Fatty Liver in Mice

Mingming Zhao,^{1,*} Lin Zhao,^{2,*} Xuelian Xiong,² Yuan He,³ Wei Huang,⁴ Zihao Liu,⁵ Liang Ji,¹ Bing Pan,¹ Xuefeng Guo,⁵ Leibo Wang,⁶ Si Cheng,⁷ Ming Xu,⁸ Hongyuan Yang,⁹ Yuxin Yin,¹⁰ Minerva T. Garcia-Barrio,¹¹ Y. Eugene Chen,¹¹ Xiangbao Meng,⁶ and Leming Zheng^{1,7}

¹The Institute of Cardiovascular Sciences and Institute of Systems Biomedicine, School of Basic Medical Sciences, Key Laboratory of Molecular Cardiovascular Sciences of Ministry of Education, NHC Key Laboratory of Cardiovascular Molecular Biology and Regulatory Peptides, Health Science Center, Peking University, Beijing, China; ²Department of Endocrinology and Metabolism, Fudan Institute of Metabolic Diseases, Zhongshan Hospital, Fudan University, Shanghai, China; ³National Research Institute for Health and Family Planning, Beijing, China; ⁴Gene Therapy Center and the Institute of Hypertension, Internal Medicine Department and Cardiovascular Division, Department of Internal Medicine, Tongji Hospital, Tongji Medical College Huazhong University of Science and Technology, Wuhan, China; ⁵Beijing National Laboratory for Molecular Sciences, State Key Laboratory for Structural Chemistry of Unstable and Stable Species, College of Chemistry and Molecular Engineering, Peking University, Beijing, China; ⁶State Key Laboratory of Natural and Biomimetic Drugs, School of Pharmaceutical Sciences, Peking University, Beijing, China; ⁷China National Clinical Research Center for Neurological Diseases, Tiantan Hospital, Advanced Innovation Center for Human Brain Protection, The Capital Medical University, Beijing, China; ⁸Department of Cardiology and Institute of Vascular Medicine, Peking University Third Hospital, Beijing, China; ⁹School of Biotechnology and Biomolecular Sciences, The University of New South Wales, Sydney, New South Wales, Australia; ¹⁰The Institute of Systems Biomedicine, Peking University, Beijing, China; and ¹¹Cardiovascular Center, Department of Internal Medicine, University of Michigan Medical Center, Ann Arbor, Michigan



See Covering the Cover synopsis on page 2018.

BACKGROUND & AIMS: Nonalcoholic fatty liver disease is characterized by excessive hepatic accumulation of triglycerides. We aimed to identify metabolites that differ in plasma of patients with liver steatosis vs healthy individuals (controls) and investigate the mechanisms by which these might contribute to fatty liver in mice. **METHODS:** We obtained blood samples from 15 patients with liver steatosis and 15 controls from a single center in China (discovery cohort). We performed untargeted liquid chromatography with mass spectrometry analysis of plasma to identify analytes associated with

liver steatosis. We then performed targeted metabolomic analysis of blood samples from 2 independent cohorts of individuals who underwent annual health examinations in China (1157 subjects with or without diabetes and 767 subjects with or without liver steatosis; replication cohorts). We performed mass spectrometry analysis of plasma from C57BL/6J mice, germ-free, and mice given antibiotics. C57BL/6J mice were given 0.325% (m/v) N,N,N-trimethyl-5-aminovaleric acid (TMAVA) in their drinking water and placed on a 45% high-fat diet (HFD) for 2 months. Plasma, liver tissues, and fecal samples were collected; fecal samples were analyzed by 16S ribosomal RNA gene sequencing. C57BL/6J mice with CRISPR-mediated disruption of the gene encoding γ -butyrobetaine hydroxylase (BBOX-knockout mice) were also placed on a 45%

HFD for 2 months. Hepatic fatty acid oxidation (FAO) in liver tissues was determined by measuring liberation of $^3\text{H}_2\text{O}$ from [^3H] palmitic acid. Liver tissues were analyzed by electron microscopy, to view mitochondria, and proteomic analyses. We used surface plasmon resonance analysis to quantify the affinity of TMAVA for BBOX. **RESULTS:** Levels of TMAVA, believed to be a metabolite of intestinal microbes, were increased in plasma from subjects with liver steatosis compared with controls, in the discovery and replication cohorts. In 1 replication cohort, the odds ratio for fatty liver in subjects with increased liver plasma levels of TMAVA was 1.82 (95% confidence interval [CI], 1.14–2.90; $P = .012$). Plasma from mice given antibiotics or germ-free mice had significant reductions in TMAVA compared with control mice. We found the intestinal bacteria *Enterococcus faecalis* and *Pseudomonas aeruginosa* to metabolize trimethyllysine to TMAVA; levels of trimethyllysine were significantly higher in plasma from patients with steatosis than controls. We found TMAVA to bind and inhibit BBOX, reducing synthesis of carnitine. Mice given TMAVA had alterations in their fecal microbiomes and reduced cold tolerance; their plasma and liver tissue had significant reductions in levels of carnitine and acyl-carnitine and their hepatocytes had reduced mitochondrial FAO compared with mice given only an HFD. Mice given TMAVA on an HFD developed liver steatosis, which was reduced by carnitine supplementation. BBOX-knockout mice had carnitine deficiency and decreased FAO, increasing uptake and liver accumulation of free fatty acids and exacerbating HFD-induced fatty liver. **CONCLUSIONS:** Levels of TMAVA are increased in plasma from subjects with liver steatosis. In mice, intestinal microbes metabolize trimethyllysine to TMAVA, which reduces carnitine synthesis and FAO to promote steatosis.

Keywords: Microbiota; NASH; Gut; Peroxisome.

Nonalcoholic fatty liver disease (NAFLD), the predominant chronic liver disease, with a prevalence of 20%–30% in Western countries,¹ is characterized by an accumulation of triglyceride (TG)-based lipid droplets due to increased peripheral lipolysis, uptake of free fatty acid (FFA) and decreased mitochondrial fatty acid oxidation (FAO).² NAFLD is a dynamic condition progressing from nonalcoholic fatty liver—simple steatosis—and through increased inflammation, hepatocyte injury, and progressive fibrosis, into nonalcoholic steatohepatitis (NASH) to finally cause cirrhosis and eventually, hepatocellular carcinoma. It can regress to isolated steatosis or smolder at a relatively constant pace towards cirrhosis. It is important to control its progression from the liver steatosis status. Despite its high prevalence and severity, effective treatments for NAFLD progression remain elusive.³

There is increased evidence supporting the central role of the microbiome in metabolic disorders, with studies trying to elucidate the functional significance of the stool microbiome in the progression of liver disease in NAFLD⁴ and other chronic liver diseases.^{5,6} Much of this evidence initially came from elegant experiments in mice showing that phenotypes could be altered through transfer of gut

WHAT YOU NEED TO KNOW

BACKGROUND AND CONTEXT

Non-alcoholic fatty liver disease (NAFLD) is characterized by excessive hepatic accumulation of triglycerides.

NEW FINDINGS

Levels of N,N,N-trimethyl-5-aminovaleric acid (TMAVA) are increased in plasma from subjects with liver steatosis. In mice, TMAVA inhibits γ -butyrobetaine hydroxylase, which reduced carnitine synthesis and fatty acid oxidation to promote steatosis.

LIMITATIONS

This study was performed using human plasma samples and mice. Further studies are needed in humans.

IMPACT

Strategies to reduce production of TMAVA by intestinal microbes might be developed for treatment of liver steatosis.

microbiota from obese animals to lean littermates.⁷ Remarkably, fecal microbiota transplantation from a patient with severe alcoholic hepatitis into mice renders them more susceptible to alcoholic liver damage with more severe liver inflammation and necrosis, as well as increased bacterial translocation.⁸

Metabolomics provide global metabolite profiles in multiple diseases, including NAFLD.⁹ Metabolic phenotyping can be used to identify biomarkers and different phenotypes of the metabolic syndrome. However, to date, many biomarkers only rest on population studies, while their associated biological mechanisms underlying the pathologies remain unknown.¹⁰ The compelling story of trimethylamine-N-oxide (TMAO) provides a methodology to research the relationship between gut flora and cardiovascular diseases.^{11,12} Specific metabolites and changes in the microbiota community and their pathophysiological contribution to NAFLD progression require more explicit characterization.¹³

Here, using metabolomics in plasma samples, we found a gut flora-generated metabolite, N,N,N-trimethyl-5-aminovaleric acid (TMAVA), which is elevated in liver steatosis and exacerbates high-fat diet (HFD)-induced fatty liver disease through increased lipolysis and inhibition of FAO due to decreased carnitine availability. The discovery of a link connecting TMAVA generation, gut microbiota

* Authors share first co-authorship.

Abbreviations used in this paper: ATGL, adipose triglyceride lipase; CI, confidence interval; FAO, fatty acid oxidation; FFA, free fatty acid; HFD, high-fat diet; NAFLD, nonalcoholic fatty liver disease; NASH, nonalcoholic steatohepatitis; TG, triglyceride; TMAO, trimethylamine-N-oxide; TMAVA, N,N,N-trimethyl-5-aminovaleric acid; TML, trimethyllysine; WT, wild-type; γ BB, γ -butyrobetaine.

 Most current article

© 2020 by the AGA Institute
0016-5085/\$36.00

<https://doi.org/10.1053/j.gastro.2020.02.033>

metabolism, and NAFLD risk has broad health-related implications.

Methods

Research Subjects

In the learning cohort, 15 patients with diagnosis of liver steatosis and 15 controls were enrolled from April 2014 to December 2014. The study was designed and carried out in accordance with the principles of the Declaration of Helsinki and approved by the Ethics Committee of Beijing TianTan Hospital. All patients provided written informed consent.

In the cross-sectional study, a total of 1157 subjects (ages 20–75 years, including healthy controls and patients with prediabetes and diabetes) who participated in annual health examinations were recruited to determine the association of gut flora-generated metabolites with their metabolic status. The study was approved by the Ethical Committee of the Chinese People's Liberation Army General Hospital and informed written consent was obtained from all subjects. See [Supplementary Material](#) for details on the inclusion and exclusion criteria.

In order to further verify the association of TMAVA and liver steatosis, an independent cross-sectional study was carried out involving a total of 767 subjects, and consisting of healthy controls and patients with liver steatosis (ages 17–80 years) randomly recruited to determine the biomarkers of liver steatosis from Zhongshan Hospital, Fudan University. This study was approved by the Ethics Committee of Zhongshan Hospital, Fudan University, and written informed consent was signed and obtained from all the participants. See [Supplementary Material](#) for details on the inclusion and exclusion criteria.

Animals and Animal Care

Starting at 5–6 weeks of age, wild-type male C57BL/6J mice were fed an HFD (45% of calories from fat, D12451; Research Diets, Inc, New Brunswick, NJ) for 8 weeks, along with the indicated interventions. BBOX-knockout mice (BBOX^{-/-}) were created using CRISPR-Cas9 in the C57BL6/J background. Five base pairs were deleted after AATGACCA in the BBOX, exon 2. All mice were housed in a specific-pathogen-free facility with a 12-hour/12-hour light/dark cycle and given free access to food and water. See [Supplementary Material](#) for details on the mouse experiments and histology. All protocols for mouse experiments were approved by the Ethics Committee of Animal Research, Peking University Health Science Center.

Metabolomics Analysis, TMAVA, and Deuterium-Labeled Syntheses, TMAVA, Quantification of TMAVA, Carnitine, γ -Butyrobetaine, Choline, and Trimethylamine-N-Oxide

See [Supplementary Material](#) for details.

Metabolic Challenges in Mice

C57BL/6J mice were administered (via gavage) the indicated stable-isotope-labeled metabolites (TML, TMAVA, γ -butyrobetaine [γ -BB], and carnitine) using a 1.5-inch 20-gauge intubation needle. The challenge gavage consisted of 150 μ L of

150 mM d9-metabolites (d9-carnitine and d9-TML, respectively) for TMAVA generation and 150 μ L of 5 μ M d9-carnitine for carnitine intestinal absorption. Plasma (50 μ L) was collected via the saphenous vein from mice at baseline and the indicated time points after gavage.¹⁴

Germ-Free Mice and Conventionalization Studies

See [Supplementary Material](#) for details on gut microbiota profiling.

Liver and Subcutaneous Adipose Tissue Proteomics

Mouse liver and subcutaneous adipose tissue were homogenized in radioimmunoprecipitation assay buffer and the protein content was determined using a Bradford protein assay kit (PA102; Biomed, Beijing, China). Protein (50 μ g) were precipitated with 4 volumes of precooled acetone and subsequently dissolved with 8M urea. See [Supplementary Material](#) for details on sample preparation and data analysis.

Detection of Affinity Between Candidate Molecules and BBOX

For the purpose of comparing the affinity between BBOX and different small molecules, Graphene Field-Effect Transistor was used as described previously. See [Supplementary Material](#) for details.

Lipolysis, Acylcarnitines, and Ceramides Extraction and Measurement, RNA Isolation and Quantitative Polymerase Chain Reaction, Adipocyte Size Determination, Fatty Acid Oxidation, and Isolation of Primary Mouse Hepatocytes

See [Supplementary Material](#) for the corresponding details.

Statistical Analysis

Statistical significance analysis was performed by 2-tailed unpaired Student *t* test followed by the demonstration of homogeneity of variance with an *F* test, or by 1-way analysis of variance (for more than 2 group comparisons) followed by Bonferroni multiple comparison post-test (GraphPad software, San Diego, CA). Otherwise, differences between 2 groups were analyzed by nonparametric test (Mann-Whitney test). Data are presented as mean \pm SEM (**P* < .05; ***P* < .01; ****P* < .001).

Results

Identification of a Metabolite, TMAVA, in Patients With Fatty Liver and Diabetes

For unbiased discovery of small-molecule metabolic profiles in plasma that predict increased risk for liver steatosis, we examined an initial cohort comprising plasma samples from 15 patients with steatosis and 15 healthy controls (see [Supplementary Methods, Figure 1A, Supplementary Table 1](#)). Untargeted liquid chromatography–mass spectrometry analysis of plasma was performed to define analytes associated with liver steatosis

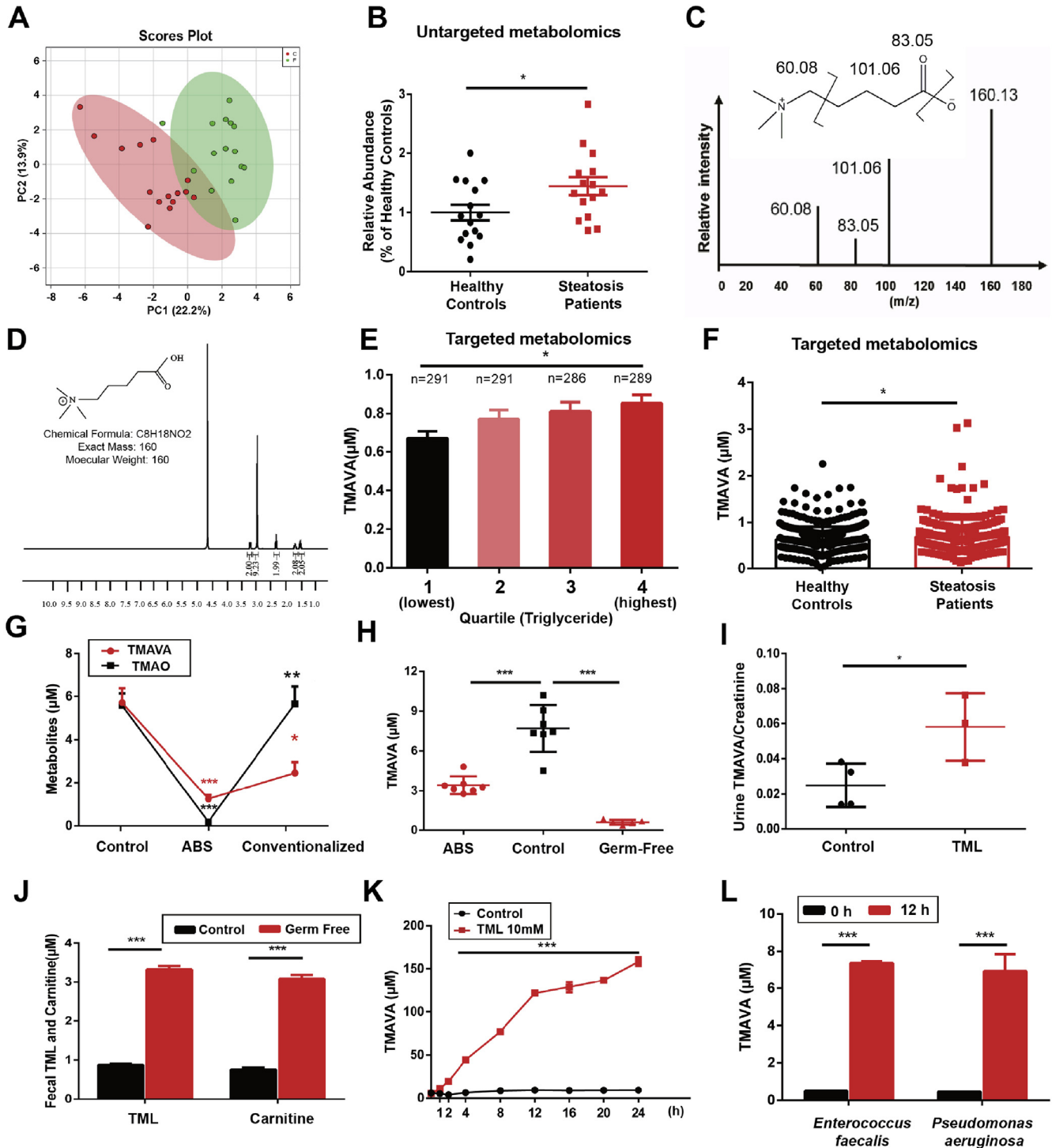
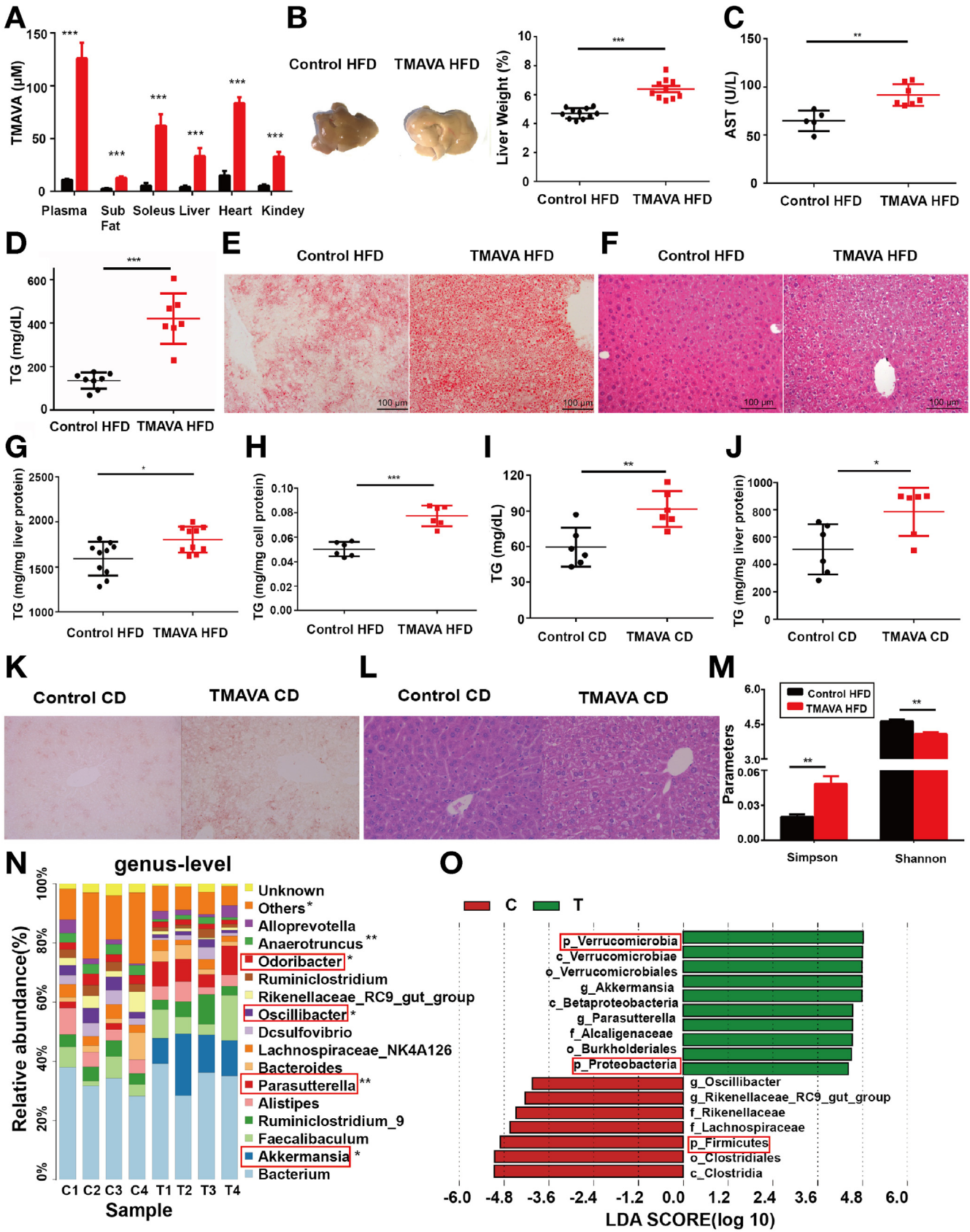


Figure 1. TMAVA is elevated in fatty liver patients and patients with diabetes and TMAVA is generated from TML through the gut flora. (A) Principal component analysis score plot of serum metabolic profiling in 15 patients with fatty liver (F) and 15 controls (C). (B) Relative abundance of TMAVA in patients with fatty liver compared with controls based on untargeted metabolomics. (C) Collision-induced dissociation mass spectrum identified TMAVA from clinical samples. (D) TMAVA identification through structural information with nuclear magnetic resonance. (E) Plasma TMAVA level in 1157 individuals that was classified by TG quartile. (F) Plasma TMAVA level was higher in patients with liver steatosis. (G) Plasma TMAVA was measured in mice after suppression of gut flora with antibiotics (ABS) (4 weeks) and subsequent placement in conventional cages with nonsterile mice (conventionalized) for 4 weeks. (H) TMAVA levels were significantly lower in plasma of germ-free mice. (I) TMAVA generation was elevated in TML-given mice. (J) TML and carnitine, were accumulated in feces in germ-free mice. (K) Feces from conventionally raised mice were co-incubated with 10 mM TML and TMAVA levels were measured at the indicated time points. (L) *Enterococcus faecalis* and *Pseudomonas aeruginosa* were co-incubated with 1 mM TML for 12 hours and TMAVA levels were measured. Statistical significance was evaluated by 2-tailed unpaired Student *t* test (B, F, and I-L) and by 1-way analysis of variance with Bonferroni multiple comparison test (E, G, and H).



(see [Supplementary Results](#), [Supplementary Tables 1 and 2](#), [Supplementary Figure 1A–D](#)). Here, we uncovered an unknown metabolite with m/z 160.1332 elevated in patients with liver steatosis ([Figure 1B](#)). We identified this liver steatosis-associated compound with an m/z of 160.1332 as TMAVA using liquid chromatography–mass spectrometry against a standard. The standard's structure was confirmed by nuclear magnetic resonance (see [Supplementary Methods](#), [Figure 1C and D](#), and [Supplementary Figure 1E](#)).

In a subsequent cross-sectional study including 1157 subjects ([Supplementary Table 3](#)), TMAVA was measured with a targeted metabolomic method and the level was significantly elevated as triglyceride levels increased (see [Methods](#), [Figure 1E](#), and [Supplementary Table 3](#)). In order to further verify the association of TMAVA with liver steatosis, an independent cohort consisting of healthy controls and patients with liver steatosis was used (see [Supplementary Methods](#) and [Supplementary Table 4](#)). Plasma TMAVA level was higher in patients with liver steatosis ([Figure 1F](#) and [Supplementary Table 4](#)). More importantly, there was a significant odd ratio for an increased risk of fatty liver with increased levels of TMAVA (odds ratio, 1.82; 95% CI, 1.14–2.90; $P = .012$) ([Supplementary Table 5](#) and [6](#)). These results indicate TMAVA is a newly identified metabolite of important prognostic value in patients with liver steatosis.

Gut Flora Is Obligatory for the Generation of the Endogenous Metabolite TMAVA

The chemical structure of TMAVA is similar to γ -BB, which is generated by the gut flora.¹⁴ Previous study found that gut flora has a contribution to the generation of trimethylated amino acids, including TMAVA.¹⁵ We found antibiotic cocktail suppressed TMAVA generation significantly, along with TMAO, a well-known cardiovascular risk factor. Then, the “conventionalized” mice (with the gut flora rescued) showed increased plasma TMAVA level (see [Supplementary Methods](#), [Figure 1G](#), and [Supplementary Figure 2A and B](#)). Germ-free mice also had trace TMAVA and TMAO levels in plasma ([Figure 1H](#), [Supplementary Figure 2C](#)). In summary, the gut flora generates TMAVA. Consistently, when mice were oral gavaged with d9-TMAVA, the anticipated d9 isotopologues of metabolites, including TMAO, were not observed, while d9-TMAO was observed after gavaged with d9-carnitine, confirming previous

reports ([Supplementary Figure 2D and E](#)).^{11,12} This suggests that the metabolic pathway of TMAVA may be different from TMAO or γ -BB.

Various microorganisms can generate 5-aminovalerate from lysine naturally employing the enzymes lysine 2-monooxygenase (DavB) and 5-aminovaleramidase (DavA).¹⁶ Plasma trimethyllysine (TML) levels were increased in patients with carotid atherosclerosis.¹⁷ We predicted that TMAVA may be generated from TML using a similar pathway to that of lysine by the gut flora. We found mice supplemented with 0.325% TML (mass/volume %) in the drinking water resulted in a 2-fold increase of TMAVA excretion in urine ([Figure 1J](#)). Additionally, TMAO precursor carnitine and TMAVA precursor TML were found to accumulate in feces of germ-free mice ([Figure 1J](#)). Moreover, when feces from conventionally raised mice were co-incubated with TML, TMAVA levels were also increased ([Figure 1K](#)). Finally, *Enterococcus faecalis* and *Pseudomonas aeruginosa* containing *davB* and *davA* were found using megablast searching (see [Supplementary Methods](#)). We co-incubated TML with *Enterococcus faecalis* and *Pseudomonas aeruginosa*, and found that TMAVA was generated ([Figure 1L](#)). Moreover, plasma TML level was also significantly higher in patients with liver steatosis ([Supplementary Table 4](#)), and there was a significant odds ratio for an increased risk of fatty liver with increased levels of TML (odds ratio, 1.33; 95% CI, 1.02–1.73; $P = .033$) ([Supplementary Table 5](#)). Collectively, these results indicate that TML serves as a precursor for gut flora-dependent formation of TMAVA.

TMAVA Treatment Exacerbates Fatty Liver and Causes Microbiota Imbalance

To investigate the underlying mechanism for the association between plasma TMAVA levels and liver steatosis risk, we fed mice with an HFD diet and TMAVA in 0.325% concentration (mass/volume %) in the drinking water for the experimental group. After 8-week TMAVA treatment, the TMAVA concentrations in plasma and various tissues showed a 10-fold increase ([Figure 2A](#)). The livers of the treated group were larger and heavier than the control livers ([Figure 2B](#)). The liver injury biomarkers in plasma showed that aspartate aminotransferase was also increased ([Figure 2C](#)). Fasting plasma TG was elevated ([Figure 2D](#)). Oil Red O staining showed that the liver tissue of the TMAVA-

Figure 2. TMAVA treatment exacerbated HFD-induced fatty liver and altered the microbiota. Mice were fed an HFD for 8 weeks, with the TMAVA group given 0.325% TMAVA (m/v %) in the drinking water in (A–H and M–O). Mice were fed a chow diet (CD) for 8 weeks, with the TMAVA group given 0.325% TMAVA (m/v %) in the drinking water in (I–L). (A) TMAVA levels in multiple tissues and plasma were measured ($n = 3$). (B) Gross appearance of the livers (*left*) and the ratio of liver weight to body weight (*right*). (C, D) Plasma aspartate aminotransferase (C) and fasting TG levels (D) ($n = 5-8$). (E, F) Oil Red O (E) and H&E (F) staining of the liver sections (original magnification 40 \times). (G) Hepatic TG contents ($n = 10$). (H) Primary hepatocytes were isolated from mice given TMAVA and TG contents were measured. (I, J) Plasma TG level (I) and hepatic TG contents (J) were measured in mice fed a CD ($n = 6$). (K, L) Oil Red O (K) and H&E (L) staining of the liver sections (original magnification 40 \times). (M) Feces were collected and the microbiota was analyzed after 8-week TMAVA treatment with HFD. Microbiota abundance was calculated using Simpson and Shannon index. (N) Comparison of proportional abundance of bacteria at the genus level in the feces of TMAVA-given (T1–T4) and control (C1–C4) mice. (O) Altered gut flora species were shown in different levels ($n = 4$). Statistical significance was evaluated by 2-tailed unpaired Student *t* test (A–D and G–J).

treated HFD group contained more lipid droplets than that of the control HFD group (Figure 2E and F). Consistent with the histologic observations, the level of the liver TG was 20% higher in TMAVA-given HFD mice (Figure 2G). An elevated TG level was also found in the primary hepatocytes isolated from 8-week TMAVA-given HFD mice compared to the hepatocytes from the HFD control (Figure 2H). To address whether TMAVA could trigger NAFLD-associated phenotypes in the absence of other challenges, mice were also given 0.325% TMAVA alone in the drinking water while on a chow diet. After 8 weeks, plasma and hepatic TG content were elevated (Figure 2I and J). Oil Red O staining showed that the liver tissue of the TMAVA-given chow group contained more lipids (Figure 2K and L). These data suggest that TMAVA could drive early steatosis in mice. Although the mice given TMAVA on chow diet had increased lipid accumulation in the liver compared to the corresponding controls within the experimental 8 weeks, liver steatosis was comparatively less than in the mice in HFD, in both control and TMAVA treatments. Therefore, we used the HFD model for liver steatosis in the subsequent experiments.

To investigate whether TMAVA treatment causes changes in the gut flora community, profiling of the microbiota composition by 16S RNA gene sequencing showed significant alterations in genes and phylum levels. The 16S functional community profiling indicated an increase in energy production and conversion, and carbohydrate transport and metabolism, and a decrease in lipid transport and metabolism (see [Supplementary Results](#), [Figure 2M–O](#), and [Supplementary Figure 3](#)). These results demonstrate a significant shift in the gut microbiota with TMAVA treatment and the alteration is closely correlated with energy metabolism.

Carnitine Biosynthesis and Fatty Acid Oxidation in Liver Are Inhibited by TMAVA

After TMAVA treatment, carnitine, which is considered to influence metabolic processes through FAO, was decreased significantly in plasma and various tissues (Figure 3A). A family of carnitine acyltransferases can convert carnitine to acylcarnitine intermediates, and plasma acylcarnitine profiling provides an integrated snapshot of in vivo substrate flux of β -oxidation.¹⁸ Consistent with the decrease in circulating carnitine, plasma and hepatic acylcarnitine species decreased significantly (Figure 3B). Liver FAO was also decreased in TMAVA-given group (Figure 3C). In addition, ultrastructural analysis uncovered that hepatic mitochondria were swollen with increased accumulation of lipid droplets and less electron-dense bodies in mice given TMAVA (Figure 3D and E). These findings suggest that hepatic mitochondria in TMAVA-given animals are dysfunctional.

The maintenance of body temperature by adipose thermoregulation utilizes energy stores in proportion to ambient temperature.¹⁹ Upon cold exposure for 6 hours at 4°C in the daylight, mice given TMAVA had lower body temperatures than control mice (Figure 3F). This phenotype

resembles that of β -adrenergic receptor-deficient mice²⁰ and adipose triglyceride lipase (ATGL)-deficient mice.²¹ It suggests that insufficient amounts of FFAs are oxidized as an energy substrate for uncoupled mitochondrial respiration upon TMAVA treatment. After cold exposure, TG and FFA were also observed to be increased in the group given TMAVA (Figure 3G and H). Notably, the molar ratio of FFAs to glycerol released was higher in mice given TMAVA (Figure 3I). After cold exposure, mice given TMAVA have elevated glucose disappearance rates, indicating that the use of glucose as an energy substrate was enhanced (Figure 3J and K). And mice given TMAVA had markedly improved glucose tolerance and altered expression of FAO-related enzymes (see [Supplementary Results](#) and [Supplementary Figure 4](#)).

TMAVA Competitively Inhibited the Binding of γ -Butyrobetaine to γ -Butyrobetaine Hydroxylase

Proteomics was employed to uncover changes in liver protein abundance and pathway activity upon TMAVA treatment. Proteins changing significantly were primarily related to the mitochondrion and peroxisomes, the locations for FAO, indicating TMAVA can regulate fatty acid metabolism (see [Supplementary Results](#), [Figure 4A–C](#), [Supplementary Figure 5A](#) and [B](#), and [Supplementary Tables 7–9](#)).

Endogenous carnitine synthesis plays an important role in physiological homeostasis.²² The rate-limiting step in this pathway involves the hydroxylation of γ -BB by γ -BB hydroxylase (BBOX) to yield carnitine (Figure 4D).²² We found that BBOX protein level in the liver was elevated with TMAVA treatment along with 8-week HFD (Figure 4E and F). And hepatic BBOX levels were highest ([Supplementary Figure 5C](#) and [D](#)). An increase in hepatic BBOX expression was observed with TMAVA treatment through proteomics, Western blot, and reverse transcriptase polymerase chain reaction (Figure 4E–G). Furthermore, more γ -BB was excreted through urine by the mice given TMAVA (Figure 4H). The decreased carnitine level and increased precursor excretion suggest that carnitine production is impaired, in spite of the BBOX being up-regulated, likely as a compensatory response. Moreover, plasma γ -BB level was also significantly higher in patients with liver steatosis ([Supplementary Table 4](#)). There was a significant odds ratio for increased risk of fatty liver with increased levels of γ -BB (odds ratio, 2.02; 95% CI, 1.25–3.27; $P = .004$) ([Supplementary Table 5](#)). To confirm the relationship between TMAVA and carnitine formation, d9- γ -BB was gavaged to control and mice given TMAVA orally. Plasma concentration of d9-carnitine generation was significantly lower in mice on chow diet after 8-week 0.325% TMAVA treatment in the drinking water (Figure 4I). Furthermore, d9-carnitine generation decreased significantly in primary hepatocytes treated with BBOX small interfering RNA (Figure 4J) or in a dose-dependent fashion with TMAVA (Figure 4K). When the BBOX protein was chemically immobilized on a graphene surface, TMAVA was able to bind BBOX with a similar profile as γ -BB, albeit with lower

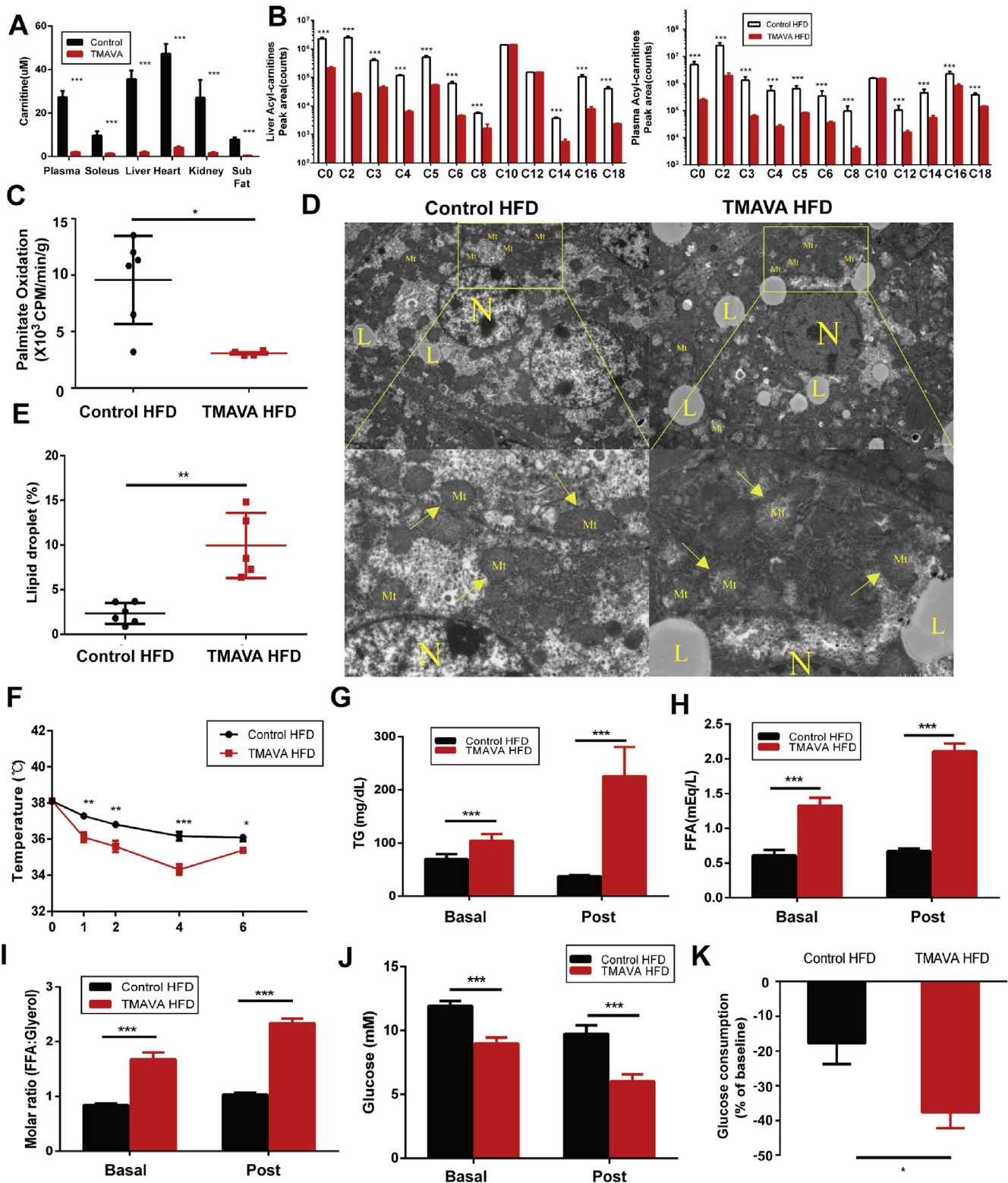


Figure 3. FAO is inhibited by TMAVA treatment. Mice were fed an HFD for 8 weeks, with the TMAVA group given 0.325% TMAVA in the drinking water (m/v %) (A–K). (A) TMAVA treatment decreased the carnitine content in plasma and various tissues. Sub fat, subcutaneous fat. (B) Acylcarnitine levels in the liver (left) and plasma (right) (n = 6 or 8). (C) Liver FAO was measured ex vivo in control and mice given TMAVA (n = 6). (D) Electron microscopy of livers. Arrows indicate swollen mitochondria with reduced density. L, lipid droplets; Mt, mitochondria; N, nuclei (original magnification 10,000×). (E) Lipid droplet percentage relative to total image horizon. Control and mice given TMAVA fed an HFD for 8 weeks were subjected to cold exposure at 4°C for 6 hours (F–K). (F) Mice rectal temperatures (n = 8). (G) Circulating TG level. (H) Circulating FFA level. (I) Molar ratio of FFAs to glycerol release. (J) Blood glucose level. Basal, before cold exposure; Post, after cold exposure. (K) Glucose consumption rates after the cold exposure. Statistical significance was evaluated by 2-tailed unpaired Student *t* test (E–K) or nonparametric test (A–C).

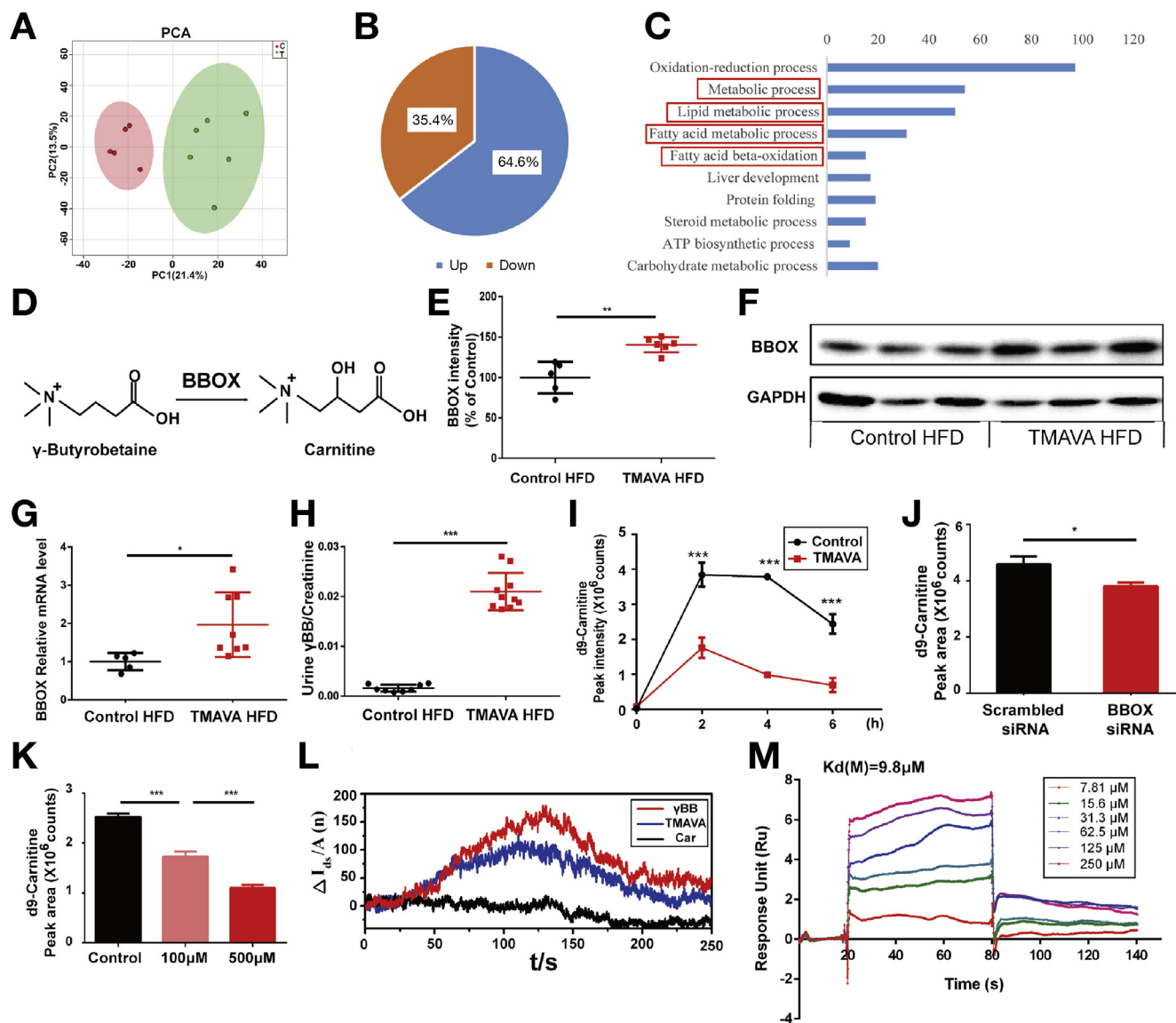


Figure 4. TMAVA inhibited the binding of γ -BB to γ -BB hydroxylase leading to carnitine synthesis inhibition. Mice were fed an HFD for 8 weeks, with the TMAVA group given 0.325% TMAVA (m/v %) in the drinking water in (A–I). (A) Comparative liver proteomics of the 2 experimental groups. Principal component analysis score plot of liver protein profiling $n = 5$ and 6. (B) The percentage of changed proteins in each group. (C) Distribution among cellular biological processes of the differentially expressed proteins. (D) Scheme for the generation of carnitine from γ -BB by BBOX catalysis. (E–G) Proteomics (E), Western blot (F), and reverse transcriptase polymerase chain reaction (G) analysis of hepatic BBOX levels. (H) γ -BB was excreted at higher levels in the urine of mice given TMAVA ($n = 8$ and 10). (I) Control and mice given TMAVA ($n = 4$) were gavaged with d9- γ -BB. d9-carnitine was measured at the indicated time points. (J) d9-carnitine generation upon BBOX small interfering RNA knockdown in HepG2 cells. (K) d9-carnitine generation upon treatment with 100 μ M and 500 μ M TMAVA in HepG2 cells for 24 hours. (L) Determination of TMAVA binding to BBOX chemically immobilized on a graphene surface. (M) Binding affinity between BBOX and TMAVA was tested using surface plasmon resonance. Statistical significance was evaluated by 2-tailed unpaired Student t test (E, G, and J–K) or nonparametric test (H and I).

affinity, suggesting that TMAVA could inhibit the binding of γ -BB to BBOX competitively (Figure 4L). The binding affinity between BBOX and TMAVA was also determined through surface plasmon resonance (Figure 4M). Additionally, wild type (WT) mice gavaged with d9-carnitine plus TMAVA had a significantly lower d9-carnitine level compared with mice gavaged with d9-carnitine alone, which indicates that TMAVA may reduce carnitine intestinal absorption (Supplementary Figure 5E and F, WT control vs

WT TMAVA). Overall, in this mouse model, TMAVA decreases the carnitine concentration in plasma and other tissues and it leads to the inhibition of FAO.

TMAVA-Treatment Causes Altered Fatty Acid Metabolism

After 8 weeks of treatment, mice fed HFD with TMAVA showed a significant lower body weight compared with the

HFD controls (Figure 5A). A reduction in fat weight may largely account for the reduced overall weight gain in mice given TMAVA (Figure 5B and C). Body composition analysis indicated that mice given TMAVA had decreased fat content without significant change in lean mass (Figure 5D). Histologic analysis showed increased percentage of small adipocytes and a lower percentage of midsize and large adipocytes in the subcutaneous fat from mice given TMAVA (Figure 5E and F). As the size of the adipocytes depends mainly on the TG accumulation, the smaller adipocyte size could be due to lower TG accumulation.

Under physiological conditions, lipids can be oxidized into energy. Excessive lipids can lead to hepatocellular damage, including liver steatosis.¹ Mice given TMAVA have higher FFA levels in blood under nonfasting and fasting conditions (Figure 5G). Plasma FFA and glycerol, which reflect lipolysis *in vivo*, were measured in the mice given TMAVA before and after administering the β 3-adrenergic receptor agonist CL-316,243.²³ FFA levels were significantly increased at both baseline and stimulated states (Figure 5H). Notably, the molar ratio of FFA to glycerol released was also higher in the group given TMAVA (Figure 5I). Glycerol release was also markedly increased *ex vivo* in fat explants from mice given TMAVA (Figure 5J). Lipolytic rates are highly regulated by hormone-sensitive lipase and ATGL.²⁴ With TMAVA treatment, mice exhibited elevated ATGL and hormone-sensitive lipase expression (Figure 5K). Cidea and UCP1 expression were also increased (Figure 5L). Adipose tissue proteomics found proteins related to FAO, especially located in peroxisomes, were up-regulated. The results suggest increased lipolysis and peroxisome activity in subcutaneous adipose tissue, resulting in brown-like characteristics (see Supplementary Results, Supplementary Figure 5G–I, and Supplementary Table 10).

The liver of TMAVA-given HFD mice showed elevated expression of fatty acid uptake genes, including CD36, FATP, and MTP (Figure 5M). In addition, mass spectrometry analysis revealed accumulated FFAs of different chain lengths in mice given TMAVA (Figure 5N). Ceramides of different chain lengths, which exert lipotoxicity in the liver, were also increased in liver (Figure 5O). Overall, these results clearly indicated that TMAVA treatment resulted in increased lipolysis in adipose tissue and ectopic accumulation of FFAs in the liver.

BBOX Deficiency Inhibits Fatty Acid Oxidation and Leads to Liver Steatosis Supporting That TMAVA Functions Through BBOX Inhibition

To address the function of BBOX in liver steatosis progression, BBOX knockout mice (BBOX^{-/-}) were created using CRISPR-Cas9. Five base pairs were deleted after AATGACCA in BBOX, exon 2 (Figure 6A and B) and no BBOX protein was detected in mice (Figure 6C). After 8-week HFD, plasma carnitine levels were decreased significantly in the BBOX^{-/-} mice and the precursor, γ -BB level was significantly elevated (Figure 6D and E). Acylcarnitine species in plasma were also markedly decreased in the knockout mice

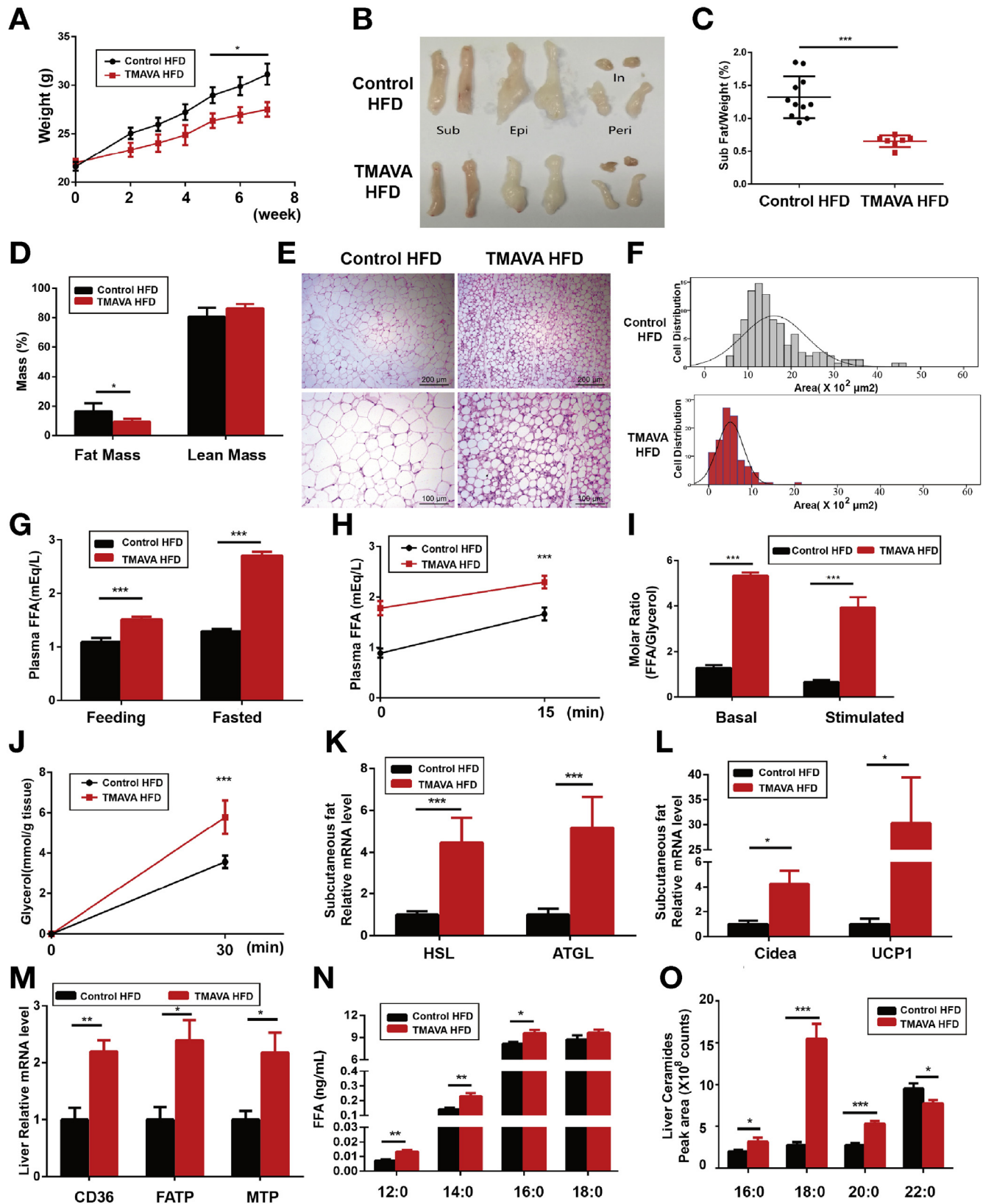
(Figure 6F). The livers of the BBOX^{-/-} group were 20% heavier and appeared paler than the control livers (Figure 6G). Plasma TG and FFA were elevated by 1-fold (Figure 6H and I). Oil Red O staining showed that the liver tissue of the BBOX^{-/-} group contained more lipid droplets (Figure 6J and K), which is consistent with our observations involving TMAVA treatment of WT mice on HFD (Figure 2). Due to decreased carnitine level, liver FAO was also decreased in the knockout mice, showing a comparable level to that of TMAVA treatment (Figure 6L vs Figure 3C). However, there was no significant difference in d9-carnitine plasma levels after gavage between WT control and BBOX^{-/-} mice within each treatment, indicating that BBOX played a negligible role in carnitine intestinal absorption (Supplementary Figure 5E and F). In summary, we found that BBOX-deficient mice in HFD have a very similar phenotype to that of WT mice treated with HFD and TMAVA, which supports that TMAVA caused fatty liver through inhibition of BBOX.

Exogenous Carnitine Supplementation Reverses TMAVA Induced Fatty Liver

To examine whether carnitine supplementation can reverse TMAVA-induced fatty liver disease, we treated mice with TMAVA supplemented with or without carnitine in their drinking water while on an HFD. Carnitine supplementation significantly reversed the TMAVA-induced decrease of carnitine in plasma (Figure 7A). The pathogenic role of TMAVA in fatty liver was significantly abolished by carnitine supplementation, as evidenced by both liver weight and aspartate aminotransferase (Figure 7B and C). Plasma TGs (Figure 7D) were reduced by 50%, to levels comparable to control mice without TMAVA treatment in HFD (Figure 2D). Plasma FFA (Figure 7E) also decreased to levels comparable to mice in HFD alone (Figure 5G). Oil Red O staining showed that the livers of carnitine-supplemented mice contained fewer lipid droplets than those of TMAVA-given HFD controls (Figure 7F and G). Consistent with the histologic observations, the amount of hepatic TG was 20% lower in carnitine-supplemented mice than in mice treated with TMAVA alone (Figure 7H). Relative messenger RNA expression of FATP and fatty acid synthesis (FASN, ACC1) genes in liver were reversed by carnitine supplementation (Figure 7I). The reduction in fat pad weight was also reversed with carnitine supplementation (Figure 7J). As a consequence, the exacerbation in fatty liver induced by TMAVA was prevented by carnitine supplementation and recovered to that observed in the HFD status without TMAVA (Figure 7K).

Discussion

Our study investigated whether there are unique endogenous metabolites that could have a profound impact on the development of fatty liver and their mechanisms of action. We presented several new findings. First, an endogenous metabolite, TMAVA, was identified and is elevated in liver steatosis patients. It was also found at higher level in patients with diabetes or liver steatosis (Figure 1A–F). We



also determined that gut flora plays an obligatory role in TMAVA generation from TML (Figure 1G–L). Second, TMAVA treatment exacerbates HFD-induced fatty liver disease in mice and alters the microbiota diversity. Also, TMAVA treatment alone can promote the formation of liver steatosis (Figure 2), which indicates TMAVA might be an independent risk factor for fatty liver. Third, TMAVA decreases carnitine level, leading to mitochondrial swelling, FAO inhibition, and resultant cold intolerance (Figure 3). TMAVA could compete with γ -BB for BBOX binding to inhibit carnitine endogenous synthesis, while simultaneously inhibiting the absorption of carnitine in the intestine (Figure 4), driving carnitine deficiency. Fourth, TMAVA causes increased lipolysis resulting in elevated FFA levels in plasma and uptake in liver (Figure 5). Fifth, BBOX deficiency inhibits FAO and leads to liver steatosis (Figure 6). Finally, carnitine supplementation alleviated the aggravated fatty liver phenotypes induced by TMAVA (Figure 7). These results indicate that gut flora and TMAVA play an important role in energy homeostasis during the eventual progression to NAFLD (Figure 7K).

We identified TMAVA as a gut flora metabolite generated from TML. Recently, a study revealed that TML levels are independently associated with incident (3-year) major adverse cardiovascular event risks and incident (5-year) mortality risk.^{25,26} TML is surprisingly abundant in both plant- and animal-derived foods,²⁵ and gut microbiota have evolved the enzymatic machinery to metabolize TML,²⁵ which is consistent with our results. Nonetheless, our studies show that in gut commensals from both mice, the capacity of TML utilization as nutrient precursor for TMAVA formation is higher compared with the conversion to TMA and TMAO.²⁵ Additionally, plasma levels of TMAO were not affected by dietary TML in that study, suggesting that TMAVA is the main metabolite from TML in the gut flora and that the deteriorative effects of TML might come from TMAVA. In patients with liver steatosis, we found that compared to subjects in the lowest quartile of TMAVA, subjects in the top quartile have elevated risk for liver steatosis (hazard ratio, 1.82; 95% CI, 1.14–2.90), suggesting that TMAVA plays an important role in NAFLD development. Additionally, plasma TML, the TMAVA precursor, was also higher in patients with liver steatosis and associated with

increased risk. Previous studies reported TMAVA is increased in pre-eclampsia patients²⁷ and diets influence TMAVA generation.^{28,29} We also found that TMAVA treatment alone can promote the formation of liver steatosis, even on a chow diet (Figure 2), which can be of high relevance both physiologically and clinically.

Carnitine is involved in long-chain fatty acid transport across the inner membrane of mitochondria for energy production.³⁰ Patients with systemic carnitine deficiency show evidence of impaired FAO associated with reduced levels of carnitine.³¹ The rate-limiting step in this pathway involves the hydroxylation of γ -BB by BBOX to yield carnitine.²² We found that TMAVA is an endogenous metabolite able to inhibit the binding of γ -BB to BBOX, leading to decreased endogenous carnitine synthesis, which, in turn, leads to a suppression in FAO (Figures 3 and 4). However, in our study, we found that plasma carnitine was increased in patients with liver steatosis, with the limitation that hepatic carnitine level could not be directly measured in our cohorts. We speculate that hepatic carnitine plays a more important role in FAO, with BBOX highly expressed in liver. This hypothesis is supported by earlier publications that explore carnitine levels, including supplementation, and NAFLD in humans.^{32–34} A previous study found that hepatic carnitine level was decreased in patients with NASH, which was consistent with a decreased mitochondrial respiratory chain complexes activity and reduced FAO in hepatocytes.³² Additionally, 2 earlier studies found that carnitine supplementation in human can benefit patients with NASH. One study³³ found that participants treated with carnitine-ornitine complex had a significantly higher rate of normalization of serum alanine aminotransferase compared with the placebo group. In another study,³⁴ patients with NASH were randomly dispensed one 1-g carnitine tablet for 24 weeks. Carnitine-treated patients showed significant improvement at the end of the study in the following parameters: aspartate aminotransferase, alanine aminotransferase, γ -glutamyltransferase, TG, and histologic scores. In agreement with these studies, we report here that carnitine supplementation reversed TMAVA-induced fatty liver disease in mice (Figure 7). In light of the new findings reported here and those initial human studies, it will be valuable to conduct carefully designed and controlled carnitine

Figure 5. TMAVA causes reduction in fat pad weight and adipocyte size, elevated FFA levels and lipolysis in vivo and ex vivo. Mice were fed an HFD for 8 weeks, with the TMAVA group given 0.325% TMAVA (m/v %) in the drinking water in (A–O). (A) Weight of mice in the control and TMAVA-given groups (n = 8). (B) Representative photographs of fat pads of mice with or without TMAVA treatment. Epi, epididymal; In, inguinal; Peri, perirenal; Sub, subcutaneous. (C) The percentage of subcutaneous fat weight to body weight in the control and TMAVA-given groups. (D) The percentage of fat mass and lean mass to body mass was detected by magnetic resonance imaging. (E) H&E-stained subcutaneous fat. Scale bar (top): 200 μ m; (bottom): 100 μ m. (F) Distribution of adipocyte size in subcutaneous fat. Each distribution was obtained from 5 mice in each group and at least 200 adipocytes from each mouse. (G) Total plasma FFA in ad libitum-fed (left) and overnight-fasted mice (right) with or without TMAVA. (H) Circulating levels of FFA in response to the β 3-adrenoreceptor agonist after 15 minutes. (I) Molar ratios of FFA to glycerol release in in vivo lipolysis. (J) Basal glycerol release in subcutaneous adipose tissue explants from control and mice given TMAVA. (K) Relative messenger RNA (mRNA) expression of hormone-sensitive lipase and ATGL in subcutaneous fat. (L) Relative Cidea and UCP1 mRNA levels (n = 6–8). (M) Relative mRNA expression of fatty acid transport proteins (n = 6). (N) Individual plasma FFA species in nonfasting conditions (n = 6–8). (O) Individual liver ceramide species in nonfasting conditions (n = 6–8). Statistical significance was evaluated by 2-tailed unpaired Student *t* test (A, C, D, G–J, and N–O) or nonparametric test (K–M).

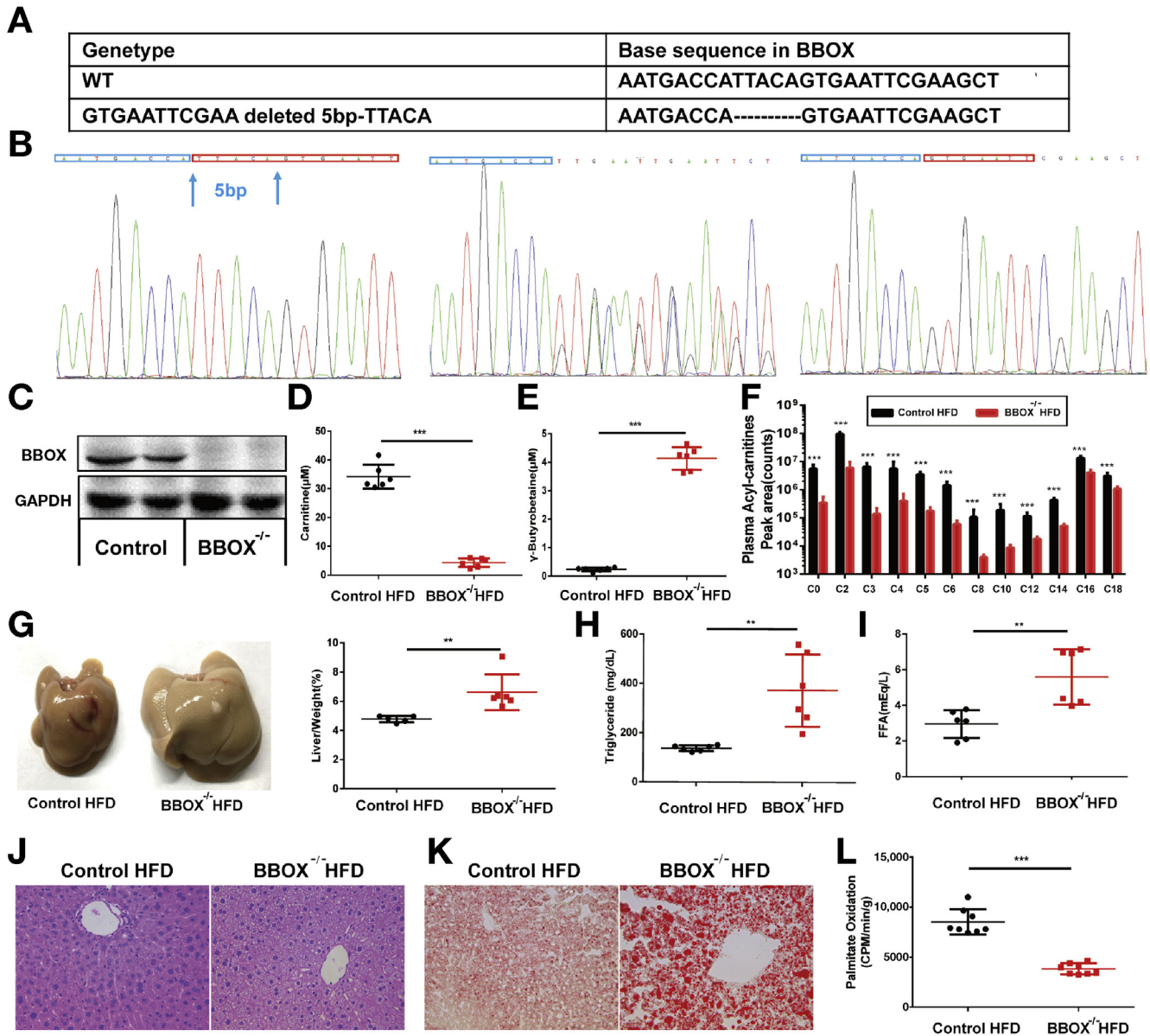


Figure 6. BBOX deficiency inhibits FAO and leads liver steatosis. WT (control) and BBOX deficient ($BBOX^{-/-}$) were fed an HFD for 8 weeks in (C–L). (A) The gene sequence of WT and knockout mice. (B) DNA sequencing of WT (left), heterozygous (*middle*) and homozygous (*right*) mice. (C) WB of BBOX protein level. (D and E) $BBOX^{-/-}$ mice display a decreased carnitine level (D) and an increased γ -BB level (E) in plasma ($n = 6$). (F) Acylcarnitine levels in the plasma of $BBOX^{-/-}$ mice ($n = 6$). (G) Gross appearance of the livers (*left*) and the percentage of liver weight to body weight. (H, I) Plasma TG (H) and FFA level (I) after 16 hours of fasting ($n = 6$). (J, K) Oil Red O (J) and H&E (K) staining of the liver sections (original magnification 40 \times). (L) Liver FAO was measured ex vivo in WT and $BBOX^{-/-}$ mice ($n = 8$). Statistical significance was evaluated by 2-tailed unpaired Student *t* test (G–I and J) or nonparametric test (D–F).

supplementation studies in follow-up randomized clinical trials including TMAVA as a marker to simultaneously address whether TMAVA can identify which patients might benefit from carnitine supplementation at different stages of NAFLD.

In this study, we found that TMAVA also decreased carnitine intestinal absorption. Therefore, carnitine deficiency in TMAVA-treated mice may be the result of simultaneous suppressed endogenous carnitine synthesis and decreased exogenous carnitine absorption. Previous study also found TMAVA can inhibit FAO through reducing

carnitine absorption by the inhibition of cell membrane carnitine transporter (OCTN2).³⁵ However, the relative contributions of these 2 sources remain to be determined. Although we found that BBOX expression was highest in the liver (Supplementary Figure 5C and D), other tissues also had some expression, albeit low (eg, cardiac tissue). Here we used conventional BBOX knockout mice because liver steatosis is intrinsically associated with whole-body metabolism. Future studies should involve liver-specific and fat-specific knockout of BBOX to evaluate the relative contribution of those tissues to BBOX-dependent TMAVA effects.

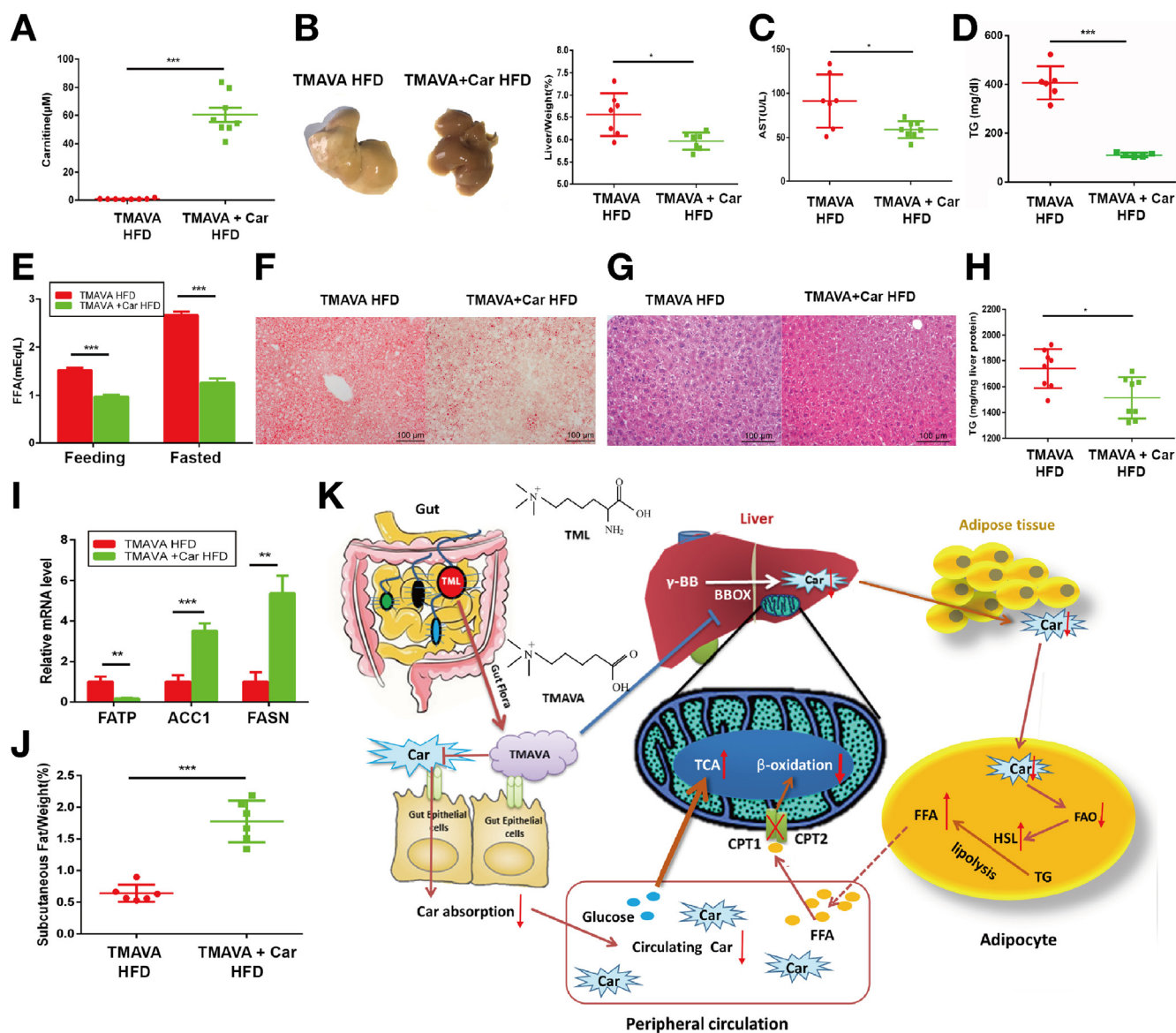


Figure 7. Exogenous carnitine supplementation reverses TMAVA-induced fatty liver. Mice given TMAVA (with 0.325% TMAVA [m/v %] in the drinking water) were fed an HFD with or without 0.325% carnitine (m/v %) in the drinking water for 8 weeks in (A–J). (A) Plasma carnitine after 8-week treatment (n = 8). (B) Gross appearance of the livers (left) and the percentage of liver weight to body weight (right). (C, D) Plasma aspartate aminotransferase level (C) and TG content (D) (n = 6–8). (E) Plasma FFA level in nonfasting and 16-hour fasting conditions (n = 8). (F, G) Oil Red O (F) and H&E (G) staining of liver sections (original magnification 40×). (H) Hepatic TG contents (n = 8). (I) Relative messenger RNA expression of fatty acid transport protein (FATP) and fatty acid synthesis (FASN, ACC1) (n = 6). (J) The ratio of subcutaneous fat weight to body weight. (K) Summary schema outlining the proposed pathway by which TMAVA promotes fatty liver. Statistical significance was evaluated by 2-tailed unpaired Student t test (B–E, H, and J) or nonparametric test (A, I).

TMAVA treatment resulted in increased lipolysis in adipose tissue and increased uptake of FFAs (Figure 5M–O) and mitochondrial dysfunction in the liver. Although our human cohorts did not have liver biopsies associated, our mouse proteomics findings are consistent with human data reported previously.³⁶ In fact, the absence of visceral and peripheral fat leads to ectopic lipid accumulation and severe hepatic and muscle insulin resistance.²³ Patients with partial lipodystrophy owing to mutations in the scaffolding protein perilipin-1, which inhibits ATGL, have reduced peripheral fat mass but develop NAFLD because of increased

adipose tissue lipolysis.³⁷ In our study, TMAVA treatment causes a reduction in fat pad weight and adipocyte size (Figure 5). Because there was carnitine deficiency in the adipose tissue (Figure 3A), this could impair FFA utilization, in spite of higher levels of circulating FFA (Figure 3H and I) to produce energy. In that scenario, energy production may shift to increase glucose utilization (Figure 3J and K) with the increase in markers of browning reflecting a compensatory mitochondrial response to increase efficiency in utilization of the limited pool of FFA substrates, albeit without being able to mount a thermogenic response (Figure 3F).²³

In conclusion, our study found that the gut flora-derived TMAVA contributes to development of NAFLD by directly affecting carnitine synthesis and subsequent FAO. The present work reveals the clinically relevant discovery that TMAVA generated by the gut flora contributes to the microbiome-dependent modulation of liver steatosis and has potential prognostic value. These studies pave the path to clinical interventions involving carnitine supplementation and flora manipulation.

Supplementary Material

Note: To access the supplementary material accompanying this article, visit the online version of *Gastroenterology* at www.gastrojournal.org, and at <https://doi.org/10.1053/j.gastro.2020.02.033>.

References

- Diehl AM, Day C. Cause, pathogenesis, and treatment of nonalcoholic steatohepatitis. *N Engl J Med* 2017; 377:2063–2072.
- Kim JK, Gavrilova O, Chen Y, et al. Mechanism of insulin resistance in A-ZIP/F-1 fatless mice. *J Biol Chem* 2000; 275:8456–8460.
- Zhang HJ, He J, Pan LL, et al. Effects of moderate and vigorous exercise on nonalcoholic fatty liver disease: a randomized clinical trial. *JAMA Intern Med* 2016; 176:1074–1082.
- Boursier J, Mueller O, Barret M, et al. The severity of nonalcoholic fatty liver disease is associated with gut dysbiosis and shift in the metabolic function of the gut microbiota. *Hepatology* 2016;63:764–775.
- Sabino J, Vieira-Silva S, Machiels K, et al. Primary sclerosing cholangitis is characterised by intestinal dysbiosis independent from IBD. *Gut* 2016;65:1681–1689.
- Qin N, Yang F, Li A, et al. Alterations of the human gut microbiome in liver cirrhosis. *Nature* 2014;513:59–64.
- Blanton LV, Charbonneau MR, Salih T, et al. Gut bacteria that prevent growth impairments transmitted by microbiota from malnourished children. *Science* 2016;351.
- Llopis M, Cassard AM, Wrzosek L, et al. Intestinal microbiota contributes to individual susceptibility to alcoholic liver disease. *Gut* 2016;65:830–839.
- Beyoglu D, Idle JR. The metabolomic window into hepatobiliary disease. *J Hepatol* 2013;59:842–858.
- Wang TJ, Larson MG, Vasan RS, et al. Metabolite profiles and the risk of developing diabetes. *Nat Med* 2011; 17:448–453.
- Koeth RA, Wang Z, Levison BS, et al. Intestinal microbiota metabolism of L-carnitine, a nutrient in red meat, promotes atherosclerosis. *Nat Med* 2013;19:576–585.
- Wang Z, Klipfell E, Bennett BJ, et al. Gut flora metabolism of phosphatidylcholine promotes cardiovascular disease. *Nature* 2011;472:57–63.
- Loomba R, Seguritan V, Li W, et al. Gut microbiome-based metagenomic signature for non-invasive detection of advanced fibrosis in human nonalcoholic fatty liver disease. *Cell Metab* 2017;25:1054–1062.e5.
- Koeth RA, Levison BS, Culley MK, et al. gamma-Butyrobetaine is a proatherogenic intermediate in gut microbial metabolism of L-carnitine to TMAO. *Cell Metab* 2014;20:799–812.
- Koistinen VM, Kärkkäinen O, Borewicz K, et al. Contribution of gut microbiota to metabolism of dietary glycine betaine in mice and in vitro colonic fermentation. *Microbiome* 2019;7:103.
- Liu P, Zhang H, Lv M, et al. Enzymatic production of 5-aminovalerate from L-lysine using L-lysine mono-oxygenase and 5-aminovaleramide amidohydrolase. *Sci Rep* 2014;4:5657.
- Skagen K, Trøseid M, Ueland T, et al. The carnitine-butyrobetaine-trimethylamine-N-oxide pathway and its association with cardiovascular mortality in patients with carotid atherosclerosis. *Atherosclerosis* 2016;247:64–69.
- Van Hove JLK, Zhang W, Kahler SG, et al. Medium-chain ceryl-CoA dehydrogenase (MCAD) deficiency: diagnosis by acylcarnitine analysis in blood. *Am J Hum Genet* 1993;52:958–966.
- Kozak LP. Brown fat and the myth of diet-induced thermogenesis. *Cell Metab* 2010;11:263–267.
- Bachman ES, Dhillon H, Zhang CY, et al. betaAR signaling required for diet-induced thermogenesis and obesity resistance. *Science* 2002;297:843–845.
- Haemmerle G, Lass A, Zimmermann R, et al. Defective lipolysis and altered energy metabolism in mice lacking adipose triglyceride lipase. *Science* 2006;312:734–737.
- Shekhawat PS, Sonne S, Carter AL, et al. Enzymes involved in L-carnitine biosynthesis are expressed by small intestinal enterocytes in mice: implications for gut health. *J Crohns Colitis* 2013;7:e197–e205.
- Liu L, Jiang Q, Wang X, et al. Adipose-specific knockout of seipin/Bscl2 results in progressive lipodystrophy. *Diabetes* 2014;63:2320–2331.
- Zechner R, Zimmermann R, Eichmann Thomas O, et al. FAT SIGNALS—lipases and lipolysis in lipid metabolism and signaling. *Cell Metab* 2012;15:279–291.
- Li XS, Wang Z, Cajka T, et al. Untargeted metabolomics identifies trimethyllysine, a TMAO-producing nutrient precursor, as a predictor of incident cardiovascular disease risk. *JCI Insight* 2018;3.
- Li XS, Obeid S, Wang Z, et al. Trimethyllysine, a trimethylamine N-oxide precursor, provides near- and long-term prognostic value in patients presenting with acute coronary syndromes. *Eur Heart J* 2019;40:2700–2709.
- Jääskeläinen T, Kärkkäinen O, Jokkala J, et al. A non-targeted LC-MS profiling reveals elevated levels of carnitine precursors and trimethylated compounds in the cord plasma of pre-eclamptic infants. *Sci Rep* 2018; 8:14616.
- Tuomainen M, Kärkkäinen O, Leppänen J, et al. Quantitative assessment of betainized compounds and associations with dietary and metabolic biomarkers in the randomized study of the healthy Nordic diet (SYSDIET). *Am J Clin Nutr* 2019;110:1108–1118.
- Kärkkäinen O, Lankinen MA, Vitale M, et al. Diets rich in whole grains increase betainized compounds associated with glucose metabolism. *Am J Clin Nutr* 2018;108:971–979.

30. Wanders RJ, Ferdinandusse S, Brites P, et al. Peroxisomes, lipid metabolism and lipotoxicity. *Biochim Biophys Acta* 2010;1801:272–280.
31. Chapoy PR, Angelini C, Brown WJ, et al. Systemic carnitine deficiency—a treatable inherited lipid-storage disease presenting as Reye’s syndrome. *N Engl J Med* 1980;303:1389–1394.
32. Perez-Carreras M, Del Hoyo P, Martin MA, et al. Defective hepatic mitochondrial respiratory chain in patients with nonalcoholic steatohepatitis. *Hepatology* 2003;38:999–1007.
33. Bae JC, Lee WY, Yoon KH, et al. Improvement of nonalcoholic fatty liver disease with carnitine-ornitine complex in type 2 diabetes (CORONA): a randomized controlled trial. *Diabetes Care* 2015;38:1245–1252.
34. Malaguamera M, Gargante MP, Russo C, et al. L-carnitine supplementation to diet: a new tool in treatment of nonalcoholic steatohepatitis—a randomized and controlled clinical trial. *Am J Gastroenterol* 2010;105:1338–1345.
35. Karkkainen O, Tuomainen T, Koistinen V, et al. Whole grain intake associated molecule 5-aminovaleic acid betaine decreases beta-oxidation of fatty acids in mouse cardiomyocytes. *Sci Rep* 2018;8:13036.
36. Kohjima M, Enjoji M, Higuchi N, et al. Re-evaluation of fatty acid metabolism-related gene expression in nonalcoholic fatty liver disease. *Int J Mol Med* 2007;20:351–358.
37. Gandotra S, Le Dour C, Bottomley W, et al. Perilipin deficiency and autosomal dominant partial lipodystrophy. *N Engl J Med* 2011;364:740–748.

Author names in bold designate shared co-first authorship.

Received June 23, 2019. Accepted February 14, 2020.

Correspondence

Address correspondence to: Lemin Zheng, PhD, The Institute of Cardiovascular Sciences and Institute of Systems Biomedicine, School of Basic Medical Sciences, Key Laboratory of Molecular Cardiovascular

Sciences of Ministry of Education, Health Science Center, Peking University, Beijing 100191, China. e-mail: zhengl@bjmu.edu.cn; fax: 0086-010-82805452.

Acknowledgments

The authors Prof Cuiqing Ma (State Key Laboratory of Microbial Technology, Shandong University) for the gift of the *DavB* and *DavA* purified proteins and Dr. Xiaohui Liu (National Protein Science Technology Center, Tsinghua University) for the assistance in untargeted metabolomics analysis. Data availability: All gut flora 16S sequence data generated or analyzed during this study are deposited in the National Center for Biotechnology Information (accession number: SRA: PRJNA507102). Additional data that support the findings of this study are available from the corresponding authors on reasonable request.

CRedit Authorship Contributions

Mingming Zhao, PhD (Conceptualization: Lead; Data curation: Lead; Formal analysis: Lead; Investigation: Equal; Methodology: Lead; Project administration: Equal; Validation: Lead; Visualization: Lead; Writing – original draft: Lead; Writing – review & editing: Equal). Lin Zhao, MD (Investigation: Equal; Methodology: Equal; Resources: Equal). Xuelian Xiong, MD (Data curation: Supporting; Investigation: Supporting; Methodology: Supporting; Resources: Supporting; Validation: Supporting). Yuan He, PhD (Data curation: Supporting; Methodology: Supporting; Writing – review & editing: Supporting). Wei Huang, PhD (Conceptualization: Supporting; Writing – original draft: Supporting). Zihao Liu, PhD (Methodology: Supporting; Writing – original draft: Supporting). Liang Ji, MD (Data curation: Supporting; Writing – original draft: Supporting).

Bing Pan, PhD (Supervision: Supporting). Xuefeng Guo, PhD (Methodology: Supporting).

Leibo Wang, MD (Methodology: Supporting). Si Cheng, PhD (Data curation: Supporting; Methodology: Supporting). Ming Xu, MD (Writing – review & editing: Supporting). Hongyuan Yang, PhD (Conceptualization: Supporting; Methodology: Supporting; Writing – review & editing: Supporting). Yuxin Yin, PhD (Writing – review & editing: Supporting).

Minerva T. Garcia-Barrio, PhD (Conceptualization: Supporting; Methodology: Supporting; Writing – review & editing: Lead). Y. Eugene Chen, PhD (Conceptualization: Supporting; Methodology: Supporting; Writing – review & editing: Equal). Xiangbao Meng, PhD (Conceptualization: Supporting; Methodology: Supporting; Writing – original draft: Supporting). Lemin Zheng, PhD (Conceptualization: Lead; Data curation: Equal; Formal analysis: Equal; Funding acquisition: Lead; Investigation: Lead; Methodology: Equal; Project administration: Lead; Resources: Lead; Supervision: Lead; Writing – review & editing: Equal).

Conflicts of interest

The authors disclose no conflicts.

Funding

This work was supported by grants 91639108, 81370235, 81770272, 81322005, 81970425, and 81970748 from the Natural Science Foundation of China. This project was also supported by the 2016YFC0903000 Grant from the Ministry of Science and Technology of China. This project was also supported by the Fundamental Research Funds for the Central Universities of China.

Supplementary Materials and Methods

Research Subjects

In the learning cohort, patients with diagnosis of liver steatosis were enrolled from April 2014 to December 2014 (Supplementary Table 1). All patients were recruited using the following inclusion criteria: aged 18–75 years; not known acute or chronic disease, except for obesity or type 2 diabetes, based on medical history, physical examination, and standard laboratory tests; and alcohol consumption <20 g/d for women and 30 g/d for men. Exclusion criteria included viral-, autoimmune-, hemochromatosis-, and drug-induced causes of liver disease. Diagnoses were established histologically in liver biopsy specimens by a single liver pathologist in each participating hospital. The study was designed and carried out in accordance with the principles of the Declaration of Helsinki and approved by the Ethics Committee of Beijing TianTan Hospital. All patients provided written informed consent.

In the cross-sectional study, a total of 1157 subjects (aged 20–75 years) (including healthy controls and patients with prediabetes and diabetes) who participated in annual health examinations were recruited to determine the association of gut flora-generated metabolites with metabolism. The participants have complete information on demographic, personal characteristics (including weight, height, and waist circumference), and clinical characteristics (including blood pressure, blood glucose, lipid concentrations, uric acid, and serum creatinine) (Supplementary Table 3). Exclusion criteria for study participation included pregnancy or lactation and a history of cancer. The study was approved by the Ethical Committee of the Chinese People's Liberation Army General Hospital and informed written consent was obtained from all subjects.

In another independent cross-sectional study, a total of 767 subjects, consisting of healthy controls and patients with liver steatosis (aged 17–80 years), were randomly recruited to determine the biomarkers of liver steatosis from those who participated in annual health examinations in Zhongshan Hospital, Fudan University. Information on demographics and clinical characteristics were collected (Supplementary Table 4). The diagnosis of fatty liver was based on ultrasonic examination. Exclusion criteria included heart, pulmonary, or renal diseases; history of alcohol abuse; and other known liver diseases. This study was approved by the Ethics Committee of Zhongshan Hospital, Fudan University and written informed consent was signed and obtained from all the participants.

Animals and Animal Care

Starting at 5–6 weeks of age, WT male C57BL/6J mice were fed an HFD (45% of calories from fat, D12451; Research Diets, Inc) for 8 weeks along with the indicated interventions. BBOX knockout mice (BBOX^{-/-}) were created using CRISPR-Cas9 in the C57BL6/J background. Five base pairs were deleted after AATGACCA in the BBOX, exon 2. All mice were housed in a specific-pathogen-free facility with a

12-hour/12-hour light/dark cycle and given free access to food and water. Core body temperature was measured with a clinical rectal thermometer (JNDA 80; China). Plasma cholesterol (180; BioSino, Beijing, China), TG (220; BioSino), and glucose (240; BioSino) were measured using enzymatic methods. Free glycerol content (E1002; Apolygen, Beijing, China) and the level of FFA were measured by a colorimetric assay (294-63601; Wako Chemical, Richmond, VA). Cold exposure was performed at 4°C, with water and food provided ad libitum. For glucose tolerance testing, mice that had been fasted for 16 hours received 2 g of glucose/kg of body weight via intraperitoneal injection. Human insulin (1 mIU/g body weight; Humulin; Eli Lilly, Indianapolis, IN) was used for insulin tolerance testing. Blood samples for glucose measurement were collected before (time 0) and at 15, 30, 60, 90, and 120 minutes after injection. Body composition was measured with an Echo MRI-100 body composition analyzer (Echo Medical Systems, Oceanside, NY). For histology, livers were sectioned at a thickness of 7 μm on a cryostat for Oil Red O staining. Paraffin-embedded white adipose tissue was sectioned at a thickness of 5 μm and stained with H&E. The data were evaluated blindly by 2 independent investigators. All mice were randomly assigned to experimental groups for further analysis. All protocols for mouse experiments were approved by the Ethics Committee of Animal Research, Peking University Health Science Center.

Metabolomics Analysis

Untargeted metabolites screening was performed on Q Exactive Orbitrap mass spectrometer (ThermoFisher, San Jose, CA) equipped with a heated electrospray ionization according to the calibrated manufacturer's guidelines. A Bridged Ethylene Hybrid Amide column was used in negative mode in liquid chromatography (LC). External mass calibration was performed before each experiment. Plasma samples were randomized in sequence and metabolites were profiled by single injection including 30 samples, 3 blanks, and 3 quality-control samples throughout the analysis. The coefficient of variation (CV) of metabolites for the same quality-control samples were <10%. The detailed parameters of the mass spectrometry (MS) instrument and LC gradient are listed in Supplementary Table 11. The resulting raw spectrogram was processed using Tracefinder 3.2 (ThermoFisher). Metabolites had 2 levels of identification, one with accurate mass matching and the other with MS/MS confirmation. Mass tolerance for database search was 8 ppm for MS and 15 ppm for MS/MS. The instrument stability was monitored using quality control samples. After peak deconvolution, alignment, integration, and normalization, a table containing retention times, exact mass pairs and normalized intensities of each variable were obtained for multivariate statistical analysis.

TMAVA and Deuterium-Labeled Syntheses

Briefly, TMAVA was prepared by gradually dissolving 20 mmol dimethylaminobutyric acid hydrochloride in dichloromethane; 22 mmol trimethylamine alcohol

(ThermoFisher) was then added dropwise at room temperature. The resulting mixture was stirred overnight. The solvent was removed in reduced pressure and the residue was used without further purification. Then the tan powder was dissolved in water to make a 10-mmol solution. Hydrochloric acid (15 mmol; ThermoFisher) were added to the reaction and the resulting solution was heated 70°C overnight. LC-MS showed that there was starting material remaining. The reaction was heated to 100°C. After 12 hours, LC-MS showed that the starting material was converted to product completely. The solvent was removed in reduced pressure and the residue was added to acetone and refluxed for 2 hours. The mixture was cooled to room temperature. After filtration, the white solid was collected. The solid was dried in reduced pressure at 40°C for 12 hours and stored at room temperature in polyethylene containers. The purity (>98%) and identity of the TMAVA synthesis were confirmed by nuclear magnetic resonance and MS. The ¹H nuclear magnetic resonance spectra were obtained in CDCl₃, d₆-DMSO, CD₃OD, or d₆-acetone at 25°C at 300 MHz or 400 MHz on an OXFORD (Varian Medical Systems, Palo, Alto, CA) with chemical shift (δ , ppm) reported relative to tetramethylsilane as an internal standard. d₉-TMAVA was synthesized with the same protocol using d₉-trimethylamine other than trimethylamine.

TMAVA Identification

The collision-induced dissociation fragment of this molecule did not match any compound recorded in the human metabolome database. To chemically define the structures of m/z 160.1332 in positive MS1 mode selected for further investigation, multiple approaches were used. First, m/z 160.1332 was imported in METLIN database and searched for matched metabolites in positive charge model with a tolerance below 30 ppm with adducts for H and Na. Methacholine was matched with characteristic fragment ion of 60.08, 101.06. Then retention time was detected with methacholine, which has a different retention time (Supplementary Figure 1F). Besides, methacholine is a drug and none of the individuals in the study were receiving this drug. The m/z of the metabolite's characteristic fragment ions includes 60.08, 83.05, and 101.06. The characteristic fragment of 60.08 (m/z) may be the trimethylamine fragment because carnitine and γ -butyrobetaine have the same fragment, shown in various diseases.¹⁻³ Additionally, there is a water molecule loss from 101.06 to 83.05, which indicated that a carboxyl may be contained in this metabolite. Therefore, a structure was speculated and synthesized named TMAVA. The same retention time and high-resolution LC-MS confirmed the identity of this metabolite.

Quantification of TMAVA, Carnitine, γ -Butyrobetaine, Choline, and Trimethylamine-N-Oxide

For liquid samples including plasma, urine, and cell medium, 20 μ L were aliquoted to a 1.5-mL tube and mixed with 80 μ L of 10 μ M internal standard composed of d₉-metabolites in methanol. For solid samples including mice

tissue, food, and feces, about 50-mg samples were ground and dissolved in 10-fold HEPES buffer (10 μ M); 20 μ L of supernatant were tested as the liquid samples. In deuterium-labeled metabolites gavage experiments, 10 μ M d₄-choline was used as internal standard. Protein in the samples was precipitated with 4-volume methanol by vortexing for 1 minute. Then the supernatant was recovered after centrifugation at 20,000g at 4°C for 10 minutes. In order to get the precise concentration of the analytes, a standard curve was performed using 20 μ L of various concentration standards (0-100 μ M) processed in parallel. Standard curves were acceptable when the coefficient of determination (R^2) reached 0.99. Supernatants (70 μ L) were analyzed by injecting onto a silica column (2.0 \times 150 mm; Luna 5u Silica 100A; cat. no. 00F-4274-B0; Phenomenex, Torrance, CA) at a flow rate of 0.5 mL/min using a LC-20AD Shimadzu pump system, SIL-20AXR autosample interfaced with an API 5500Q-TRAP mass spectrometer (AB SCIEX, Framingham, MA). A discontinuous gradient was generated to resolve the analytes by mixing solvent A (0.1% propanoic acid in water) with solvent B (0.1% acetic acid in methanol) at different ratios starting from 2% B linearly to 95% B over 5.0 minutes, then hold for 1.0 minutes, and then back to 2% B. Analytes were monitored using electrospray ionization in positive-ion mode with multiple reaction monitoring of precursor and characteristic product-ion transitions of TMAVA at m/z 160.1 \rightarrow 83, d₉-TMAVA at m/z 169.1 \rightarrow 83, TMAO at m/z 76 \rightarrow 58, d₉-TMAO at m/z 85 \rightarrow 66, choline at m/z 104 \rightarrow 59.8, d₉-choline at m/z 113.2 \rightarrow 68.9, d₄-choline at m/z 108.1 \rightarrow 59.8, carnitine at m/z 162.1 \rightarrow 103, d₉-carnitine at m/z 171.1 \rightarrow 102.8, γ -BB at m/z 146.1 \rightarrow 87, d₉- γ -BB at 155.1 \rightarrow 69, respectively. Three quality-control samples with different TMAVA concentrations were measured every 20 samples. The standard curve of TMAVA is presented in Supplementary Figure 1G. The accuracy of TMAVA concentration and CV% of quality controls were calculated and were listed in Supplementary Table 6.

Production of TMAVA from Trimethyllysine

DavB and DavA purified from *E. coli* BL21(DE3) carrying the plasmids pETDuet-davB or pETDuet-davA were a gift from Cuiqing Ma (State Key Laboratory of Microbial Technology, Shandong University).⁴ DavB and DavA were coupled for TMAVA production from TML. A typical coupled reaction was carried out in a 1.5-mL sterile tube with 500 μ L reaction broth containing 100 mM phosphate buffer (pH 7.4), 5g/L L-lysine, 1 mg/mL DavB, and 1 mg/mL DavA. The reaction was conducted at 37°C with 200 rpm shaking. Samples (20 μ L) were taken at the indicated times and TMAVA was measured with LC-MS.

Lipolysis

For in vivo lipolysis, mice were fasted for 4 hours and given an intraperitoneal injection of the specific β -adrenergic receptor agonist CL-316,243 (0.1 mg/kg; Sigma-Aldrich, St Louis, MO). Blood was collected before and 15 minutes after injection for determination of FFA and glycerol levels.⁵ For ex vivo lipolysis, epididymal fat was

removed and cut into 100 mg fat pads as described by Liu et al.⁶ The medium was collected for determination of glycerol levels.

Analysis of Liver Lipids

Liver (about 100 mg wet weight) was weighed and homogenized in 1 mL of phosphate-buffered saline. Lipids were extracted as described by Folch et al⁷ and dissolved in 1 mL of 3% Triton X-100. Triglycerides and total cholesterol were measured using enzymatic methods, as described previously.⁶

Free Fatty Acid, Acylcarnitines, and Ceramides Extraction and Analysis

For the measurement of acylcarnitines in plasma, 200 μ L of acetonitrile (ACN) was added to 15 μ L of plasma, then vortexed and centrifuged for 15 minutes at 12,000 rpm. The supernatant was subjected to MS. Mobile phase A was prepared with 5 mM ammonium acetate in 95% ACN. Mobile phase B was prepared with 5 mM ammonium acetate in 5% ACN, and the pH was adjusted to 9.0 with ammonium hydroxide solution. Plasma FFA and ceramides were extracted in 400 μ L of 2:1 chloroform: methanol for 100 μ L plasma. The mixture was vortexed and centrifuged for 15 minutes at 12,000 rpm. The lower chloroform layer was collected and dried under nitrogen. Then, the lyophilized powder was dissolved in 20 μ L of 1:1 methanol:chloroform and 60 μ L of 2:1:1 isopropanol:ACN:water. Lipid extraction from the tissue samples was as described above except that tissues were homogenized beforehand. Then, the levels were normalized to the protein concentrations, which were measured using a Bradford assay. Mobile phase A was prepared with 10 mM ammonium acetate in 60% acetonitrile with 0.5% formic acid. Mobile phase B was prepared with 10 mM ammonium acetate in isopropanol/ACN in a 9:1 solution with 0.1% formic acid. The multiple reaction monitoring list of metabolites is provided in [Supplementary Table 12](#).

Germ-Free Mice and Conventionalization Studies

Mice were kept under strict light–dark cycles, with lights being turned on at 6 AM and turned off at 6 PM. For antibiotic treatment, an antibiotic cocktail (0.5 g/L vancomycin, 1 g/L neomycin sulfate, 1 g/L metronidazole, and 1 g/L ampicillin) previously shown to be sufficient to deplete all detectable commensal bacteria was administered in the drinking water, which was available ad libitum.³ Four weeks later, antibiotic-given mice were “conventionalized” by placement in cages with mice not given antibiotics or through fecal transplantation experiments. For fecal transplantation, stool samples from conventional mice were collected fresh from individual mice. Two hundred milligrams of stool were resuspended in 1 mL of phosphate-buffered saline, homogenized and filtered through a 70- μ m strainer. Recipient mice were given 400 μ L of the filtrate by gavage every day for the first week.⁸

Megablast Searching

By using megablast algorithm to compare the *davB* and *davA* gene sequences, about 100 sequences from taxonomy

bacteria in the database aligned to the query sequence. Most of them belong to *Gamma proteobacteria*, *Pseudomonas*, *Pseudomonas putida* group, while other belong to *Stenotrophomonas rhizophila* and *Enterococcus faecalis*. We found 2 close bacteria with >80% identity, *Enterococcus faecalis* and *Pseudomonas aeruginosa*, with *davB* and *davA*.

Metabolic Challenges in Mice

C57BL/6j mice were administered (by gavage) the indicated stable-isotope-labeled metabolites (TML, TMAVA, γ -BB, and carnitine) using a 1.5-inch 20-gauge intubation needle. The challenge gavage consisted of 150 μ L of 150 mM d9-metabolites (d9-carnitine, d9-TML, respectively) for TMAVA generation and 150 μ L of 5 μ M d9-carnitine for carnitine intestinal absorption. Plasma (50 μ L) was collected via the saphenous vein from mice at baseline and the indicated time points after gavage.¹

Gut Microbiota Profiling

Fresh feces samples were snap-frozen in liquid nitrogen and stored at -80°C . Genomic DNA was extracted from the colonic content samples (0.25 g) using a PowerSoil DNA Isolation Kit (MO BIO Laboratories, Carlsbad, CA). Total genome DNA from samples was extracted via the sodium dodecyl sulfate method.⁹ The concentration and purity of the extracted DNA were measured using a Nanodrop spectrophotometer (ND-1000; NanoDrop Technologies, Wilmington, DE). The V3–V4 region of the bacterial 16S ribosomal RNA gene was amplified by polymerase chain reaction (PCR) (95°C for 5 minutes, followed by 25 cycles of 95°C for 30 seconds, 50°C for 30 seconds, 72°C for 40 seconds, and 72°C for 7 minutes) using the primers 338F (5'-CTCCTACGGGAGGCAGCA-3') and 806R (5'-GGACTACHVGGGTWTCTMAVAT-3'). The PCR products were mixed with the same volume of 2X loading buffer and were separated by electrophoresis on 1.8% agarose gel for detection. Samples with a bright main band of approximately 450 bp were chosen and mixed in equi-density ratios. Then, the mixture of PCR products was purified using a GeneJET Gel Extraction Kit (Thermo Scientific).

The 16S ribosomal RNA gene amplicons were used to determine the diversity and structural comparisons of the bacterial species in mice gut microbiota using Illumina HiSeq sequencing at Biomarker Bioinformatics Technology Co Ltd (Beijing, China). Sequencing libraries were measured using an Agilent 2100 bioanalyzer following the manufacturer's recommended protocol. The qualified libraries were amplified on cBot to generate the cluster on the flow cell. Paired-end reads were allocated to samples based on their unique barcode. The overlapping regions between the paired-end reads were merged using FLASH, version 1.2.7. Sequences were removed if they were shorter than 200 nucleotides, longer than 1000 nucleotides, or contained primer mismatches, ambiguous bases, uncorrectable barcodes, and homopolymer runs in excess of 6 bases. The chimera sequences were detected by comparing tags with the reference database (Gold database) using the UCHIME

algorithm and then removed. The remaining sequences were analyzed using the open source software package Quantitative Insights into Microbial Ecology (QIIME, version 1.8.0). Sequences with $\geq 97\%$ similarity were grouped into the same operational taxonomic units (OTUs). The relative abundances of bacteria at each taxonomic level (eg, phylum, class, order, family, and genus) were computed for each mouse. α - (Simpson and Shannon), β -Diversity and principal coordinate analysis based on unweighted Unifrac distances were conducted by QIIME.

RNA Isolation and Quantitative Real-Time Polymerase Chain Reaction

Total RNA was isolated from mouse tissues using TRIzol reagent (Invitrogen, Carlsbad, CA) as per the manufacturer's instructions. Messenger RNA (mRNA) levels were quantified by quantitative PCR with SYBR Green (Invitrogen). Complementary DNA was synthesized from 5 μg of DNaseI-treated total RNA using SuperScript II reverse transcriptase (Invitrogen). Samples were normalized against 18S mRNA levels. Primers are listed in [Supplementary Table 13](#).

Adipocyte Size Determination

Subcutaneous fat samples were fixed in 10% buffered formalin, embedded in paraffin, cut into 5- μm -thick sections and stained with H&E. Five separate fields from 4 different mice were quantified using a Leica DM IRB microscope (Leica, Wetzlar, Germany).⁶

Fatty Acid Oxidation

Hepatic FAO was determined by the liberation of $^3\text{H}_2\text{O}$ from [^3H] palmitic acid according to a procedure described previously,¹⁰ with minor modifications to accommodate for the fact that liver samples were used. The reaction mixture was Krebs-Ringer bicarbonate buffer containing 74KBq/mL 9,10(n)-[^3H] palmitic acid (1.96TBq/mmol; NET043001MC; PerkinElmer, Waltham, MA) and 4% bovine serum albumin (fatty acid free; Applygen), which was aerated with 5% CO_2 -95% O_2 gas for at least 20 minutes before use. Liver slices (approximately 10 mg) were incubated with the reaction mixture for 1 hour at 30°C. After the incubation period, a 2-M KCl-HCl solution was added to the reaction mixture to stop the reaction. The resulting mixture was washed with CHCl_3 -methanol (2:1) to remove the lipids, including the undesired radioactive materials. The radioactivity of the aqueous phase was counted with a liquid scintillation counter (Tri-Carb 2500; Perkin-Elmer).¹¹

Liver and Subcutaneous Adipose Tissue Proteomics

Mouse liver and subcutaneous adipose tissue were homogenized in radioimmunoprecipitation assay buffer and the protein content was determined using a Bradford protein assay kit (PA102; Biomed). Fifty micrograms protein was precipitated with 4 volumes precooled acetone and redissolved with 8M urea. Proteins were reduced by 10 mM dithiothreitol and alkylated by 50 mM iodoacetamide. The

protein was digested in solution using sequencing grade trypsin (Promega, Madison, WI) at 37°C overnight. The digested peptides were desalted and dried in a SpeedVac Concentrator (ThermoFisher Scientific). Peptides were suspended in 0.1% formic acid and subjected to nano-LC-MS/MS analysis. The data-dependent mass spectra were acquired with LTQ Orbitrap Elite mass spectrometer (ThermoFisher Scientific) equipped with a nano-electrospray ion source (ThermoFisher Scientific). Raw mass spectra files were processed with Proteome Discoverer 1.4 (ThermoFisher Scientific) and searched in the human Uniprot database (version 2017_01) through the SEQUEST search engine. The precursor ion mass tolerance was set to 10 ppm, and MS/MS tolerance 0.02 Da.

Affinity of Candidate Molecules with BBOX

For the purpose of comparing the affinity between BBOX and different small molecules, Graphene Field-Effect Transistor was used as described previously.^{12,13} Briefly, Graphene Field-Effect Transistor is a novel method base on monitoring the drain-source current flow induced by the gate effect of a charged small molecule. BBOX was chemically immobilized on the graphene surface so that the molecular binding process could be detected.

Isolation of Primary Mouse Hepatocytes

Hepatocytes were isolated by a 2-step collagenase perfusion of the liver as described previously.¹⁴ Briefly, mice were anesthetized with 1% pentobarbital. The catheter was placed into hepatic portal vein and used to perfuse KRG containing 100 μM EGTA, followed by perfusion of KRG containing 0.5 mg/mL collagenase and 2 mM CaCl_2 . The entire digested liver was clipped, the fascia was torn with tweezers, and the liver cells released. The suspension was sieved with a 70- μm cell strainer and centrifuged 4 minutes at 50g per minute twice with cold Dulbecco's modified Eagle medium containing 10% fetal bovine serum. Cells were counted and seeded at the appropriate cell density, according to the specific experimental designs.

Electron Microscopy Analysis

For routine electron microscopy, microslicer sections of the liver (100 μm) and very thin razor blade sections of liver were prepared and fixed for 15 minutes with 1% glutaraldehyde in 0.1 mol/L PIPES buffer (pH 7.4), washed briefly in 0.1 mol/L PIPES buffer, postfixed with reduced osmium, and embedded in Epon 812.¹⁵

Statistical Analysis

Statistical significance analysis was performed by 2-tailed unpaired Student *t* test followed by the demonstration of homogeneity of variance with an *F* test, or by 1-way analysis of variance (for more than 2 group comparisons) followed by Bonferroni multiple comparisons post-test (GraphPad software). Otherwise, differences between 2 groups were analyzed by nonparametric test (Mann-Whitney test). Data are presented as mean \pm SEM.

Data Availability

All gut flora 16S sequence data generated or analyzed during this study were deposited in the National Center for Biotechnology Information (accession number: SRA:

PRJNA507102). Additional data that support the findings of this study are available from the corresponding authors on reasonable request.

Supplementary Results

Untargeted Metabolomics Found Pathways Were Changed in Patients With Fatty Liver and Controls

One hundred and three metabolites were examined (Supplementary Table 2) and patients showed a significantly altered metabolic profile compared with controls in principal component and heatmap analyses (Figure 1A, Supplementary Figure 1A–C). As in other NAFLD populations, the most significant changes were observed on amino acids (glutamine and valine) and lipid metabolites (glycerophosphorylcholine and acylcarnitines), consistent with previous studies (Supplementary Table 2).^{16,17} Ingenuity Pathway Analysis revealed that aminoacyl-transfer RNA biosynthesis, nitrogen metabolism, and the glutamine and glutamate metabolism pathway were changed significantly (Supplementary Figure 1D).

TMAVA Causes Major Alteration of the Microbiota in High-Fat Diet Mice

To investigate whether TMAVA treatment causes changes in the gut flora community, we collected feces from HFD-fed mice given with or without TMAVA for 8 weeks. Profiling of the microbiota composition by 16S RNA gene sequencing followed by principal component analysis based on OTUs showed significant alterations of the microbiota content in feces samples from mice given TMAVA (Supplementary Figure 3A). Increased Simpson's index and decreased Shannon's index showed decreased microbiota diversity in the group given TMAVA (Figure 2M). Average-neighbor method was employed to confirm that both the individual species and genus-based hierarchical clustering were significantly changed in the microbiota composition and the clustering of the fecal samples from the groups given TMAVA (Supplementary Figure 3B and C). *Firmicutes* and *Bacteroidetes* were the top 2 most abundant phyla both in groups given TMAVA and the HFD control (50.69% and 40.30%, respectively) (Supplementary Figure 3D). We observed differences in OTU abundance at the genus level. *Oscillibacter* and *Odoribacter* were decreased in groups given TMAVA, while *Akkermansia* and *Parasutterella* were increased (Figure 2N). Analysis at the phylum level indicated that *Firmicutes* decreased while *Proteobacteria* and *Verrucomicrobia* increased in the group given TMAVA (Figure 2O). The 16S functional community profiling was carried out using clusters of orthologous groups of proteins, which indicated an increase in energy production and conversion, and carbohydrate transport and metabolism, and a decrease in lipid transport and metabolism

(Supplementary Figure 3E). These results demonstrate a significant shift in the gut microbiota with TMAVA treatment and the alteration is closely correlated with energy metabolism.

However, mouse models have intrinsic limitations and do not faithfully recapitulate human disease. In this study, mice had surprisingly higher plasma TMAVA levels than those found human patients (5–10 μM vs 0.5–1 μM) at baseline, which further increased by approximately 10-fold upon oral administration of TMAVA, likely reflecting species-specific metabolic differences. It should be noted that the 10-fold increase (Figure 3A) in plasma TMAVA in mouse after 8 weeks of TMAVA oral treatment was comparable to that observed for TMAO upon pharmacologic administration of TMAO.³ Our experimental design is comparable to that study, with pharmacologic administration of TMAVA and HFD in a relatively short-term accelerated disease model, as opposed to the chronic effects of long-term exposure to gut flora-derived metabolites in normal disease progression in human.

TMAVA Altered Liver Fatty Acid Oxidation

After cold exposure, mice given TMAVA have elevated glucose disappearance rates, indicating that the use of glucose as an energy substrate was enhanced. Consistent with this, after 8-week TMAVA treatment, mice given TMAVA had markedly improved glucose tolerance, as well as improved insulin tolerance (Supplementary Figure 4A and B). Regarding FAO inhibition, the expression of FAO genes, including *CPT1a*, *CPT1b*, *CPT2*, *Acadm*, *Acadl*, and *Acadvl*, were increased in the liver tissue of mice given TMAVA. Mice given TMAVA showed suppressed expression of lipogenic genes, including *FASN*, *ACC1*, *ACC2*, and stearoyl-coenzyme A desaturase, in a metabolically compensatory pattern (Supplementary Figure 4C and D).

Proteomics was employed to uncover changes in liver protein abundance and pathway activity upon TMAVA treatment. The TMAVA-given HFD-fed mice showed a significantly altered proteomic profile compared with the HFD controls (Figure 4A). A total of 2529 proteins were examined, and 443 of these proteins changed significantly, with 64.6% proteins down-regulated and 35.4% up-regulated (Figure 4B). The liver proteome indicated cellular processes related to metabolism were changed, especially in fatty acid metabolism (Figure 4C, Supplementary Figure 5A, and Supplementary Table 7). The enrichment analysis of GO cellular components also revealed that the proteins were mainly (38.5%) localized in the mitochondrion (Supplementary Figure 5B and Supplementary Table 8). Functional cluster analysis revealed that the proteins changing significantly were

primarily related to the mitochondrion and peroxisomes, the locations for FAO. These cell organelles can regulate lipid metabolism and oxidation-reduction processes (Supplementary Table 9).

TMAVA Altered Adipose Fatty Acid Oxidation

In order to shed light on the mechanisms driving these responses, adipose tissue proteomics were performed. The TMAVA-given HFD-fed mice showed a significantly altered proteomic profile compared with the HFD controls (Supplementary Figure 5G). The adipose proteome indicated that cellular processes related to metabolism were changed, especially oxidation-reduction process and mitochondrial electron transport, which were changed significantly in cellular process analyses (Supplementary Figure 5H). Protein functional clustering of the adipose proteomics indicated that the changed proteins were primarily related to the mitochondrion (Supplementary Table 10). The levels of FAO proteins, including peroxisomal bifunctional enzyme (Ehhadh), Acad very long chain (Acadvl), catalase (Cat), and Peroxisomal acyl-coenzyme A oxidase 1 (Acox1) were increased in the adipose tissue of mice given TMAVA. While the levels of gluconeogenesis-related proteins, including pyruvate carboxylase and glucose-6-phosphate 1-dehydrogenase X

were decreased (Supplementary Figure 5J). These results suggest increased lipolysis and peroxisome activity in subcutaneous adipose tissue resulting in brown-like characteristics.

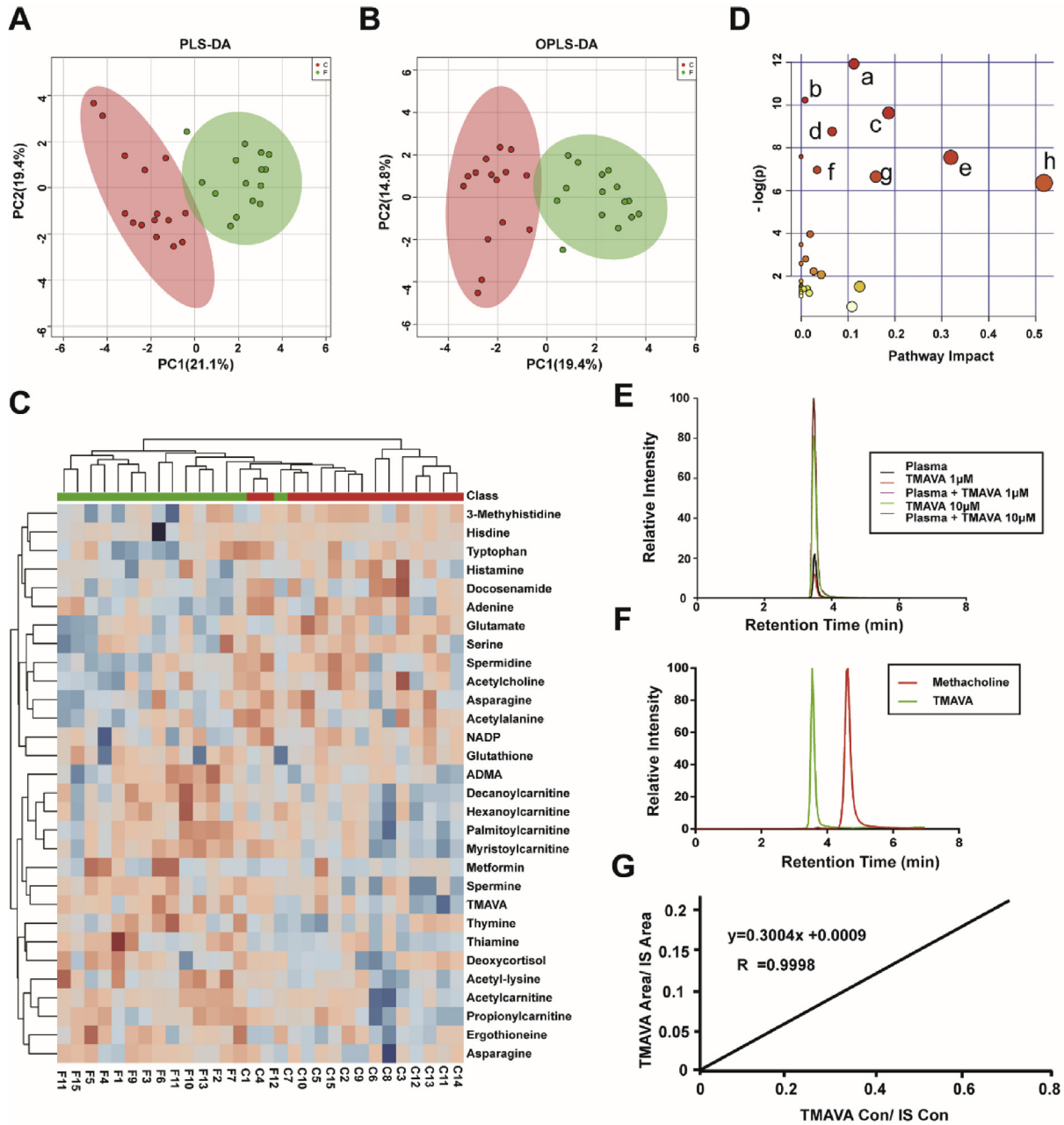
The expression of FAO genes was also up-regulated especially, in peroxisome. These phenotypes were concurrent with increased brown-like fat characteristics; yet, they are at odds with the finding that the mice given TMAVA present impaired thermogenesis. It is possible that, because there was carnitine deficiency in the adipose tissue (Figure 3A), this could impair FFA utilization, in spite of higher levels of circulating FFA (Figure 3H and I) to produce energy. In that scenario, energy production may shift to increase glucose utilization (Figure 3J and K) with the increase in markers of browning reflecting a compensatory mitochondrial response to increase efficiency in utilization of the limited pool of FFA substrates, albeit without being able to mount a thermogenic response (Figure 3F).⁶ Increased peroxisomal activity could also compensate for the reduced FAO (Supplementary Figure 5J). The contribution of adipose tissue metabolism to NAFLD deserves further attention, particularly because the observation that may contribute independently of insulin resistance¹⁸ and the recent demonstration that gut flora can control thermogenesis.¹⁹

Supplementary References

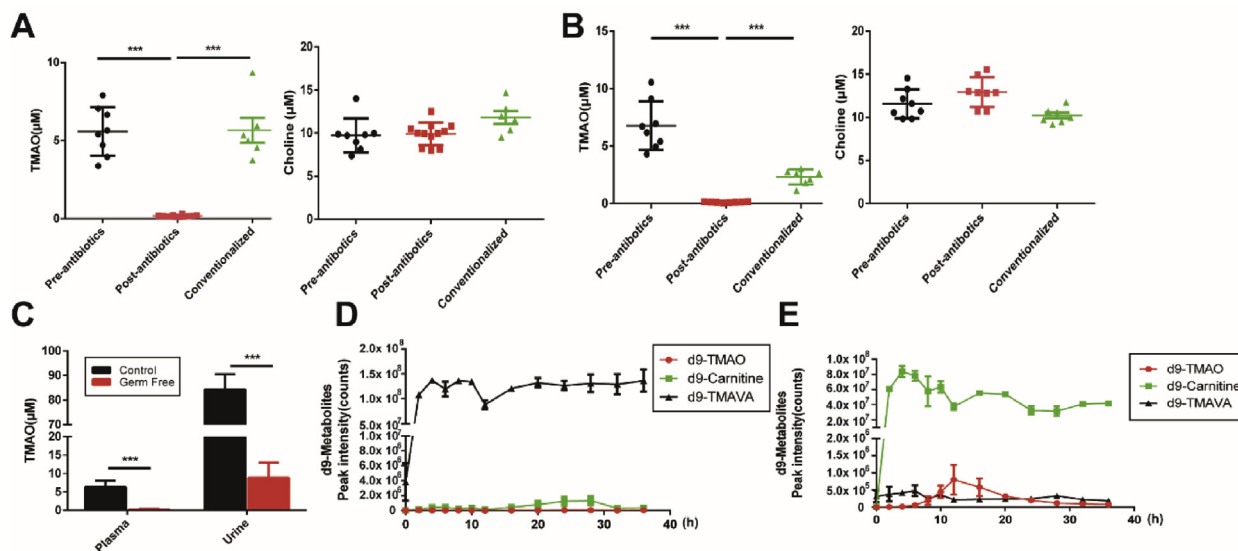
1. Koeth RA, Levison BS, Culley MK, et al. Gamma-butyrobetaine is a proatherogenic intermediate in gut microbial metabolism of L-carnitine to TMAO. *Cell Metab* 2014;20:799–812.
2. Koeth RA, Wang Z, Levison BS, et al. Intestinal microbiota metabolism of L-carnitine, a nutrient in red meat, promotes atherosclerosis. *Nat Med* 2013;19:576–585.
3. Wang Z, Klipfell E, Bennett BJ, et al. Gut flora metabolism of phosphatidylcholine promotes cardiovascular disease. *Nature* 2011;472:57–63.
4. Liu P, Zhang H, Lv M, et al. Enzymatic production of 5-aminovaleate from L-lysine using L-lysine mono-oxygenase and 5-aminovaleamide amidohydrolase. *Sci Rep* 2014;4:5657.
5. Chen W, Chang B, Saha P, et al. Berardinelli-seip congenital lipodystrophy 2/seipin is a cell-autonomous regulator of lipolysis essential for adipocyte differentiation. *Mol Cell Biol* 2012;32:1099–1111.
6. Liu L, Jiang Q, Wang X, et al. Adipose-specific knockout of seipin/Bscl2 results in progressive lipodystrophy. *Diabetes* 2014;63:2320–2331.
7. Folch J, Lees M, Sloane Stanley GH. A simple method for the isolation and purification of total lipides from animal tissues. *J Biol Chem* 1957;226:497–509.
8. Zhu W, Gregory JC, Org E, et al. Gut microbial metabolite TMAO enhances platelet hyperreactivity and thrombosis risk. *Cell* 2016;165:111–124.
9. Natarajan VP, Zhang X, Morono Y, et al. A Modified SDS-based DNA extraction method for high quality environmental DNA from seafloor environments. *Front Microbiol* 2016;7:986.
10. Araki O, Ying H, Zhu XG, et al. Distinct dysregulation of lipid metabolism by unliganded thyroid hormone receptor isoforms. *Mol Endocrinol* 2009;23:308–315.
11. Harada N, Oda Z, Hara Y, et al. Hepatic de novo lipogenesis is present in liver-specific ACC1-deficient mice. *Mol Cell Biol* 2007;27:1881–1888.
12. Fu W, Jiang L, van Geest EP, et al. Sensing at the surface of graphene field-effect transistors. *Adv Mater* 2017;29.
13. Xu S, Zhan J, Man B, et al. Real-time reliable determination of binding kinetics of DNA hybridization using a multi-channel graphene biosensor. *Nat Commun* 2017;8:14902.
14. Kao CY, Factor VM, Thorgeirsson SS. Reduced growth capacity of hepatocytes from c-myc and c-myc/TGF-alpha transgenic mice in primary culture. *Biochem Biophys Res Commun* 1996;222:64–70.
15. Ibdah JA, Paul H, Zhao Y, et al. Lack of mitochondrial trifunctional protein in mice causes neonatal hypoglycemia and sudden death. *J Clin Invest* 2001;107:1403–1409.
16. Alonso C, Fernández-Ramos D, Varela-Rey M, et al. Metabolomic Identification of Subtypes of Nonalcoholic Steatohepatitis. *Gastroenterology* 2017;152:1449–1461.e7.

17. **Lehmann R, Franken H**, Dammeier S, et al. Circulating lysophosphatidylcholines are markers of a metabolically benign nonalcoholic fatty liver. *Diabetes Care* 2013;36:2331–2338.
 18. Santoro N, Kursawe R, D'Adamo E, et al. A common variant in the patatin-like phospholipase 3 gene (PNPLA3) is associated with fatty liver disease in obese children and adolescents. *Hepatology* 2010; 52:1281–1290.
 19. **Li B, Li L**, Li M, et al. Microbiota depletion impairs thermogenesis of brown adipose tissue and browning of white adipose tissue. *Cell Rep* 2019;26:2720–2737.e5.
-

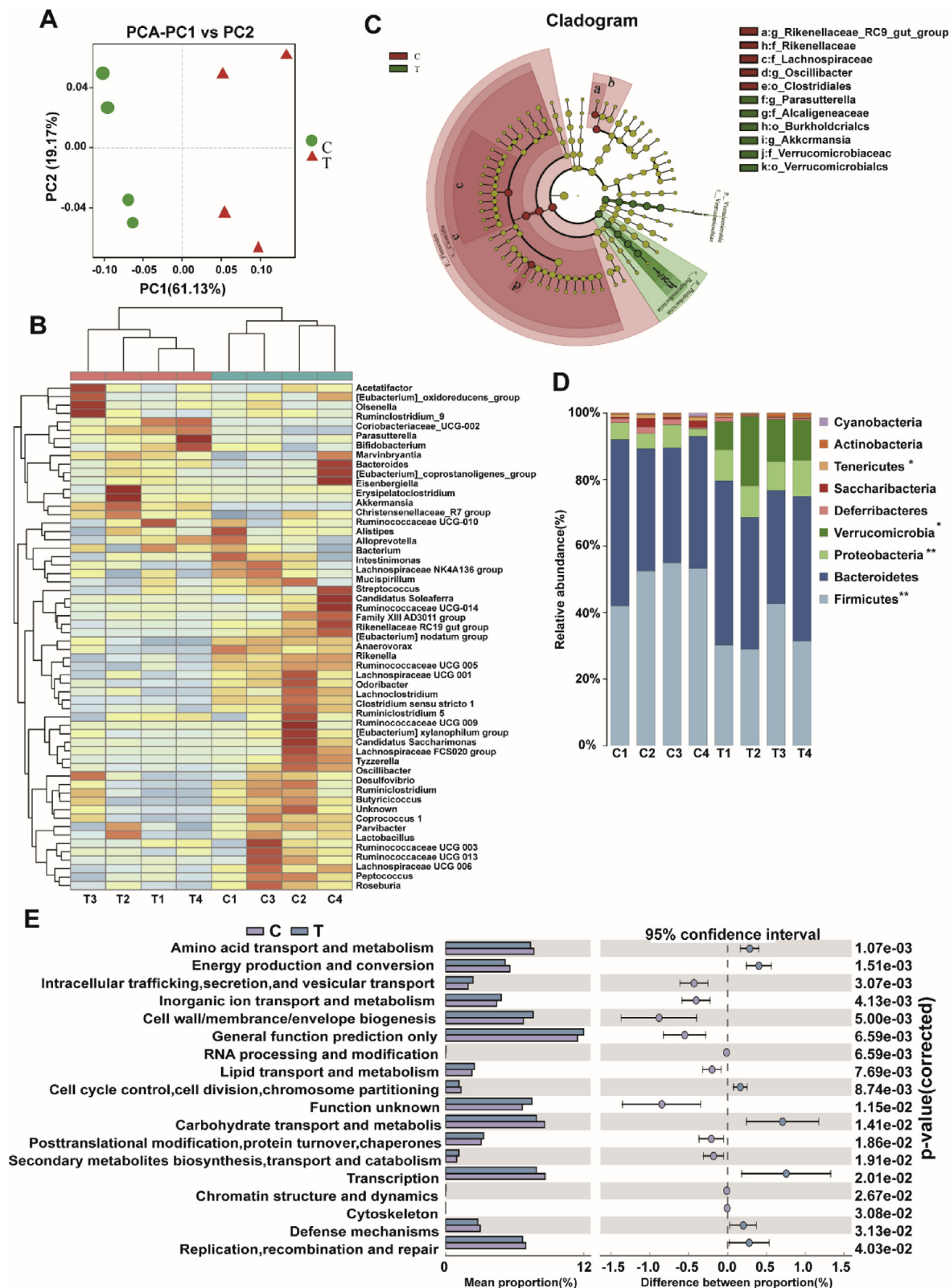
Author names in bold designate shared co-first authorship.



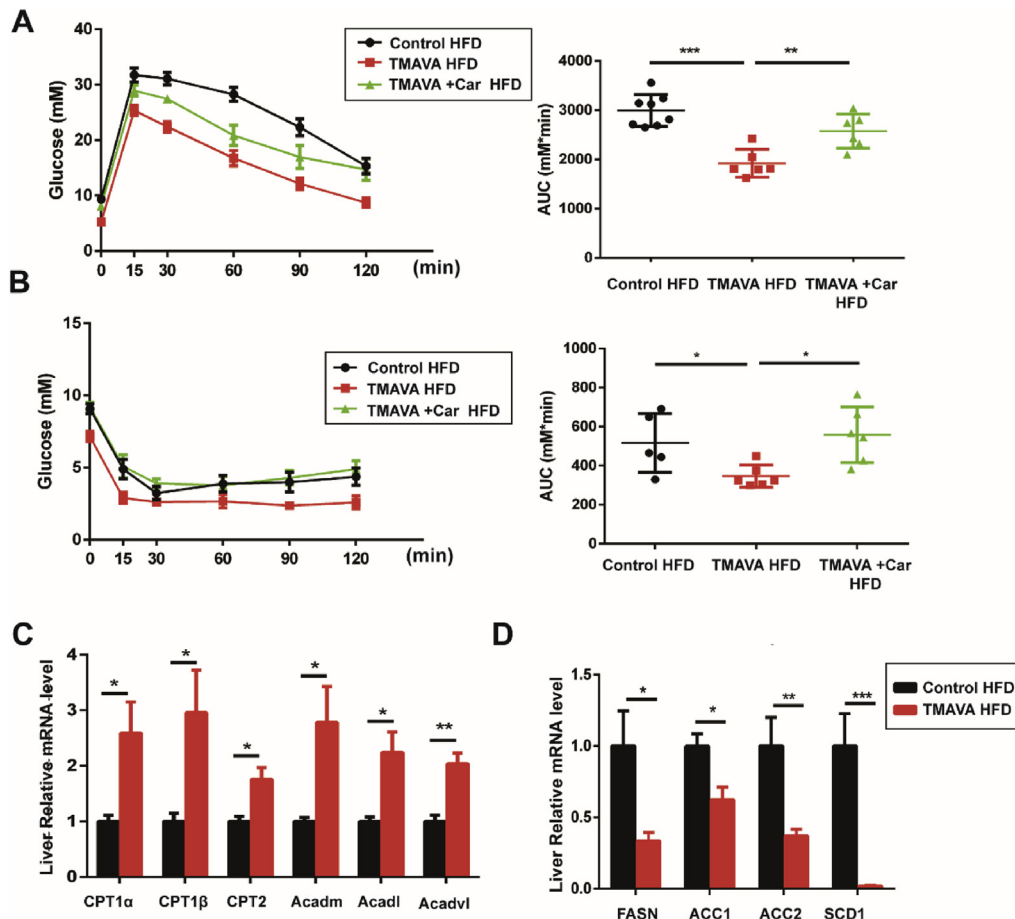
Supplementary Figure 1. Multivariate statistical analysis of plasma metabolic profiling in patients with fatty liver and controls; identification and quantification of TMAVA. (A) Partial least squares discriminant analysis (PLS-DA) of plasma metabolic profiling in 15 patients with fatty liver and 15 controls using MetaboAnalyst. C, control; F, fatty liver. (B) Orthogonal partial least squares discriminant analysis (OPLS-DA) of plasma metabolic profiling in 15 patients with fatty liver and 15 controls using MetaboAnalyst. C, control; F, fatty liver. (C) Hierarchical cluster analysis heatmaps of differential plasma metabolite levels between fatty liver patients and controls. Red indicates up-regulation and blue indicates down-regulation. The columns and rows represent experimental plasma samples and metabolites, respectively. (D) Metabolomics pathway analysis (MetPA) of disrupted metabolic pathways in fatty liver patients based on plasma samples: (a) aminoacyl-transfer RNA biosynthesis; (b) nitrogen metabolism; (c) histidine metabolism; (d) β -alanine metabolism; (e) glutamate metabolism; (f) arginine and proline metabolism; (g) glycine, serine, and threonine metabolism; and (h) alanine, aspartate, and glutamate metabolism. The color represents the P value of the indicated pathway. The circle size represents the impact of the indicated pathway. (E) TMAVA alone or plasma spiked with different concentrations of TMAVA were measured with MS. (F) Different retention times of LC-MS analyses of methacholine and TMAVA standards. (G) Standard curves for LC-MS/MS analysis of TMAVA: 80 μ L of 10 μ M d9-TMAVA internal standard in methanol were added to 20 μ L of different concentrations of the TMAVA standard.



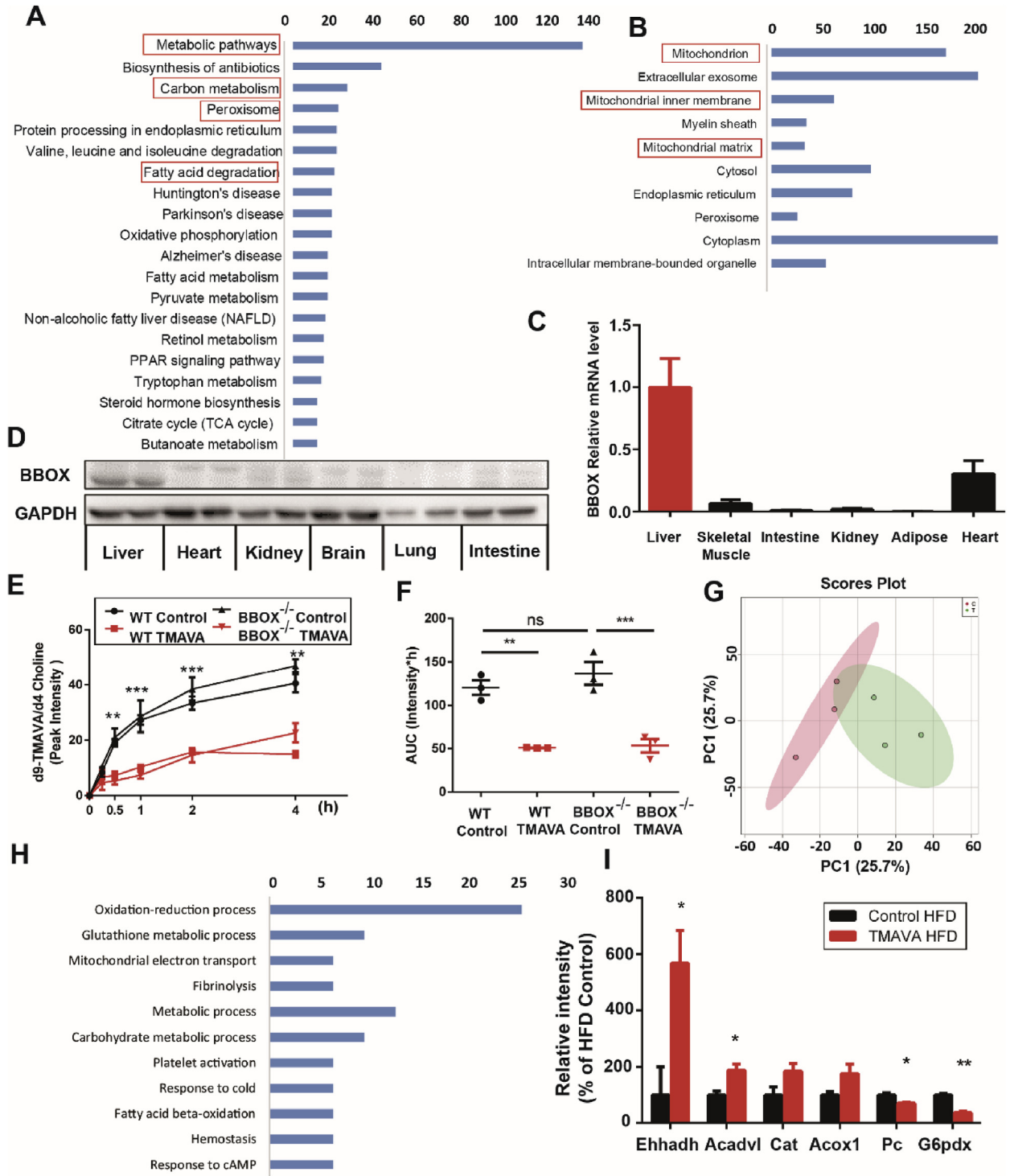
Supplementary Figure 2. TMAVA is generated independently of carnitine or TMAO. (A, B) Plasma levels of TMAO (positive control) (*left*) and choline (negative control) (*right*) in mice after suppression of gut flora with an antibiotic cocktail (4 weeks) and subsequent placement (4 weeks) in conventional cages with nonsterile mice (“conventionalized”) (A) or after fecal transplantation (B) (see Methods). (C) TMAO was decreased in plasma and urine in germ-free mice ($n = 3$). (D) Mice were gavaged with $150 \mu\text{L}$ of 150 mM d9-TMAVA. Measurement of d9-carnitine, d9-TMAVA, and d9-TMAO were performed in serial venous blood draws at the indicated times by stable isotope dilution LC-MS/MS. (E) Mice were gavaged with $150 \mu\text{L}$ of 150 mM d9-carnitine. Measurement of d9-carnitine, d9-TMAVA, and d9-TMAO were performed as in (D). Statistical significance was evaluated by 1-way analysis of variance with Bonferroni multiple comparison test (A, B) ($***P < .001$). Data are expressed as mean \pm SEM.



Supplementary Figure 3. TMAVA causes major alteration of the microbiota in HFD mice. Mice were fed an HFD for 8 weeks, with the TMAVA group given 0.325% TMAVA (m/v %) in the drinking water in (A–E). (A) Principal component analysis (PCA) was performed for the gut microbiome profiles of the fecal samples (n = 4). (B) Heatmaps generated using R language are shown. (C) Alternative gut flora at the phylum, class, order, family, genus, and species levels according to the proportions of OTUs. p, phylum, c, class, o, order, f, family, g, genus, s, species (n = 4). (D) Comparison of phylum-level proportional abundance of bacteria in the feces of TMAVA-given and control mice. (E) 16S functional gene prediction was carried out using clusters of orthologous groups of proteins.



Supplementary Figure 4. TMAVA treatment protected mice from diet-induced obesity and insulin resistance. Mice were fed an HFD for 8 weeks, with the TMAVA group given 0.325% TMAVA (m/v %) in the drinking water and the carnitine group given 0.325% TMAVA (m/v %) + 1.3% carnitine (m/v %) in (A–D). (A) Results of glucose tolerance test (GTT) (left) were quantified as area under the curve (AUC) (right). (B) Results of insulin tolerance test (ITT) (left) were quantified as AUC (right) ($n = 5-8$). (C) Reverse transcriptase quantitative polymerase chain reaction (RT-qPCR) analysis of hepatic mRNA expression of lipid oxidation genes after TMAVA treatment. (D) RT-qPCR analysis of hepatic mRNA expression of lipogenic genes after TMAVA treatment. Acadl; Acad long chain; Acadm, acyl-CoA dehydrogenase medium chain, Acadvl, Acad very long chain; ACC, acetyl-CoA carboxylase; CPT, carnitine palmitoyltransferase; FASN, fatty acid synthase; SCD, stearoyl-coenzyme A desaturase. Statistical significance was evaluated by 1-way analysis of variance with Bonferroni multiple comparison test (A, B) or nonparametric test (C, D) (* $P < .05$; ** $P < .01$; *** $P < .001$). Data are expressed as mean \pm SEM.



Supplementary Figure 5. TMAVA increases baseline lipolysis and inhibits carnitine biosynthesis and absorption. Mice were fed an HFD for 8 weeks, with the TMAVA group given 0.325% TMAVA (m/v %) in the drinking water in (A, B, and G–I). (A) Distribution of enriched proteins among cellular components in the proteomics analysis. (B) The pathways associated with the enriched proteins were identified using KEGG analysis. (C) Relative basal BBOX mRNA levels in various tissues from mice in chow diet (n = 3). Expression level was determined by reverse transcriptase quantitative polymerase chain reaction and normalized to 18S expression. (D) Relative basal BBOX protein levels in various tissues from mice in chow diet. Mice were gavaged with 200 μ L of 5 mM d9-carnitine alone or 5 mM d9-carnitine and 500 mM TMAVA. (E) Measurement of d9-carnitine was performed in serial venous blood draws at the indicated time points by stable isotope dilution LC-MS/MS (** and *** for comparison of WT Control and WT TMAVA). (F) Results for d9-carnitine were quantified as area under the curve (AUC). (G) Comparative adipose tissue proteomics of the 2 experimental groups. Principal component analysis score plot of adipose protein profiling. (H) Distribution among cellular biological processes of the differentially expressed proteins. (I) Relative intensity of subcutaneous adipose proteins related to FAO from the proteomics analysis. Acadvl, Acad very long chain; Acox1, peroxisomal acyl-coenzyme A oxidase 1; Cat, catalase; Ehhadh, peroxisomal bifunctional enzyme; G6pdx, glucose-6-phosphate 1-dehydrogenase X; Pc, pyruvate carboxylase. Statistical significance was evaluated by 1-way analysis of variance with Bonferroni multiple comparison test (F) or nonparametric test (E) and (I) (* P < .05; ** P < .01; *** P < .001). Data are expressed as mean \pm SEM.

Supplementary Table 1. Baseline Characteristics of Patients With Liver Steatosis in the Learning Cohort

| Characteristic | Healthy controls (n = 15) | Patients with liver steatosis (n = 15) |
|----------------------------------|---------------------------|--|
| Male, % | 53.3 | 33.3 |
| Blood glucose, <i>mmol/L</i> | 5.866 ± 0.498 | 6.955 ± 0.756 |
| Total cholesterol, <i>mmol/L</i> | 4.278 ± 0.356 | 4.384 ± 0.276 |
| Triglycerides, <i>mmol/L</i> | 1.718 ± 0.329 | 2.244 ± 0.362 |
| HDL cholesterol, <i>mmol/L</i> | 0.9527 ± 0.0465 | 1.056 ± 0.0765 |
| LDL cholesterol, <i>mmol/L</i> | 2.605 ± 0.370 | 2.590 ± 0.205 |
| BUN, <i>mmol/L</i> | 4.955 ± 0.226 | 5.629 ± 0.404 |
| ALT, <i>U/L</i> | 13.86 ± 2.502 | 21.23 ± 3.416 |
| AST, <i>U/L</i> | 14.19 ± 1.947 | 19.93 ± 3.177 |
| Uric acid, <i>μmol/L</i> | 310.3 ± 24.17 | 360.1 ± 17.09 |
| Creatinine, <i>μmol/L</i> | 58.03 ± 3.493 | 64.68 ± 2.812 |
| Creatine kinase, <i>U/L</i> | 73.86 ± 13.73 | 87.01 ± 8.937 |

ALT, alanine transaminase; AST, alanine transaminase; BUN, blood urea nitrogen; HDL, high-density lipoprotein; LDL, low-density lipoprotein.

Supplementary Table 2. Untargeted Metabolite Profiling in Individuals With and Without Liver Steatosis

| Compound name | <i>P</i> value | Fold (control/patients) |
|--|----------------|-------------------------|
| Acetylcarnitine | .001936 | 2.11925 |
| Glycerophosphocholine | .002859 | 0.635704 |
| Palmitoyl-L-carnitine | .003341 | 1.389989 |
| Dodecanoylcarnitine (low) | .008311 | 0.614237 |
| Myristoylcarnitine | .008769 | 1.521973 |
| (R)-(+)-2-Pyrrolidone-5-carboxylic acid | .009656 | 0.872086 |
| Decanoyl-L-carnitine | .01123 | 1.98841 |
| Spermine | .016398 | 1.230636 |
| Hexanoylcarnitine | .016989 | 1.58462 |
| Adenine | .018017 | 0.820373 |
| Histidine | .022165 | 0.784883 |
| Glutamine | .022308 | 0.889501 |
| 3-Methyl-L-histidine | .023063 | 0.735327 |
| L-Asparagine | .028003 | 0.854594 |
| Betaine | .028711 | 0.865616 |
| L-Valine | .028711 | 0.865616 |
| N,N,N-trimethyl-5-aminovaleric acid | .033945 | 1.443078 |
| Guanine | .035986 | 1.733231 |
| Propionylcarnitine | .038078 | 1.383932 |
| 1-O-(cis-9-Octadecenyl)-2-O-acetyl-sn-glycero-3-phosphocholine | .047386 | 0.821166 |
| Serine | .051431 | 0.88797 |
| Homoserine | .053447 | 0.866576 |
| Asymmetric dimethylarginine | .055408 | 1.13777 |
| Imidazoleacetic acid | .057075 | 1.227472 |
| Thymine | .057075 | 1.227472 |
| Histamine | .057572 | 0.810387 |
| Tryptophan | .073945 | 0.913513 |
| Metformin | .079122 | 10.73742 |
| N-Acetyl-L-alanine | .080221 | 0.902162 |
| Glutathione | .083767 | 1.388261 |
| 21-Deoxycortisol | .089932 | 1.754713 |
| Aspartic acid | .089952 | 1.516884 |
| Acetylcholine | .090155 | 0.862293 |
| Cytosine | .103266 | 0.912975 |
| 2-Methylbutyroylcarnitine | .118451 | 1.241602 |
| Proline | .123979 | 0.81043 |
| Cys-Gly | .133544 | 0.656249 |
| Ornithine | .146742 | 0.867526 |
| Hypoxanthine | .184607 | 1.413989 |

Supplementary Table 2. Continued

| Compound name | P value | Fold (control/patients) |
|--|---------|-------------------------|
| Deoxyinosine | .19407 | 2.021877 |
| Docosenamide | .214128 | 1.308565 |
| Methionine | .226714 | 0.82966 |
| Pantothenic acid | .227083 | 0.766818 |
| Phytosphingosine (low) | .239984 | 0.968533 |
| Inosine | .240403 | 2.303181 |
| Thymidine | .257845 | 1.135989 |
| Linoleoyl ethanolamide | .28096 | 1.454236 |
| Adenosine | .308406 | 1.19536 |
| Deoxyguanosine | .308406 | 1.19536 |
| Riboflavin (vitamin B-2) | .336274 | 1.472704 |
| S-Adenosylmethionine | .345597 | 0.620192 |
| Cystine | .358099 | 0.899687 |
| Cytidine diphosphate choline | .393959 | 0.794923 |
| Tyrosine | .411178 | 0.917648 |
| Deoxycytidine | .421494 | 0.684532 |
| ADP | .454183 | 1.463516 |
| Pipecolic acid | .472033 | 0.958052 |
| Niacinamide (low) | .476002 | 1.08439 |
| N-acetyl-L-glutamic acid | .477247 | 1.102948 |
| Citrulline | .479682 | 0.926982 |
| 3-Hydroxypicolinic acid (low) | .479773 | 0.854251 |
| 2'-O-Methyladenosine | .497457 | 1.123405 |
| Phosphocholine | .515551 | 0.966408 |
| Uridine | .523426 | 0.919366 |
| Uridine monophosphate | .523786 | 0.898506 |
| Cystathionine | .535367 | 0.750503 |
| Xanthine | .542245 | 1.277649 |
| Uracil | .56702 | 0.934026 |
| 7-Methylguanine (low) | .570573 | 1.035368 |
| Carnitine | .583283 | 1.02468 |
| Deoxyadenosine | .600289 | 1.132707 |
| Glutamate | .603319 | 1.051529 |
| Lysine | .624707 | 0.97056 |
| Eicosanoyl-EA (low) | .62961 | 1.017946 |
| L-Homocysteic acid | .660805 | 0.978909 |
| Creatinine | .682715 | 0.977108 |
| Creatine | .705627 | 0.938495 |
| Taurine | .709444 | 1.047551 |
| Aminobutyric acid | .757331 | 0.92304 |
| N-Methylglutamic acid | .764983 | 1.05263 |
| Sphingosine | .773558 | 0.988668 |
| 4-Guanidinobutanoic acid | .78894 | 0.970992 |
| N1-Acetylspermidine | .789871 | 0.975994 |
| 5-Aminosalicylic acid | .793946 | 1.070401 |
| Thiamine monophosphate | .801472 | 1.026836 |
| Ribothymidine (low) | .805304 | 0.964857 |
| L-Isoleucine | .844266 | 1.011678 |
| L-Leucine | .844266 | 1.011678 |
| Saccharopine | .856708 | 1.051597 |
| Palmitic amide | .897161 | 0.960414 |
| Guanosine | .899093 | 0.976641 |
| Butyryl-L-carnitine/isobutyryl carnitine | .903761 | 1.01355 |
| Choline | .906121 | 1.007047 |
| Carnosine | .906647 | 0.970184 |
| Pyridoxine (vitamin B-6) | .910796 | 1.056788 |
| Oleamide | .917885 | 1.039368 |
| Arginine | .925637 | 0.992506 |
| N2-Acetyl-L-ornithine | .938129 | 1.015836 |
| Phenylalanine | .979366 | 1.002032 |
| Adenosine monophosphate | .986307 | 0.994082 |

Supplementary Table 2. Continued

| Compound name | <i>P</i> value | Fold (control/patients) |
|-------------------|----------------|-------------------------|
| Acetyl-CoA | .988615 | 1.003625 |
| Sphinganine | .991864 | 1.00028 |
| D-Glutamylglycine | .995711 | 0.999454 |

ADP, adenosine diphosphate; CoA, coenzyme A.

Supplementary Table 3. Baseline Characteristics of Patients With Metabolic Syndrome in the Targeted Metabolomics Study

| Characteristic | Total (N = 1157) |
|---|------------------|
| Age, <i>y</i> , mean (IQR) | 46.0 (38.0–52.0) |
| Male, % | 65.2 |
| BMI, <i>kg/m</i> ² , mean (IQR) | 27.6 (25.8–29.4) |
| Systolic BP, <i>mmHg</i> , mean (IQR) | 129 (118–139) |
| Diastolic BP, <i>mmHg</i> , mean ± SD | 82 ± 12 |
| Blood glucose, <i>mmol/L</i> , mean (IQR) | 5.7 (5.2–6.6) |
| Total cholesterol, <i>mmol/L</i> , mean (IQR) | 5.3 (4.6–5.9) |
| Triglycerides, <i>mmol/L</i> , mean (IQR) | 1.8 (1.2–2.7) |
| HDL cholesterol, <i>mmol/L</i> , mean (IQR) | 1.2 (1.1–1.4) |
| LDL cholesterol, <i>mmol/L</i> , mean (IQR) | 2.8 (2.4–3.2) |
| Uric acid, <i>mg/dL</i> , mean ± SD | 372.5 ± 98.0 |
| Creatinine, <i>mg/dL</i> , mean (IQR) | 70.2 (61.2–81.2) |
| Hypertension, % | 33.7 |
| Dyslipidemia, % | 52.2 |
| Hyperuricemia, % | 34.4 |

BMI, body mass index, BP, blood pressure; HDL, high-density lipoprotein; IQR, interquartile range. LDL, low-density lipoprotein.

Supplementary Table 4. Baseline Characteristics of Patients With Liver Steatosis in the Independent Cohort

| Characteristic | Healthy (n = 494) | Fatty liver disease (n = 273) |
|-------------------------------|----------------------|-----------------------------------|
| Sex, male/female, n | 219/275 | 207/66 |
| Age, y | 45 (37–53) | 49 (42–56) |
| Fasting blood glucose, mmol/L | 4.89 (4.5–5.1) | 5.1 (4.7–5.7) |
| ALT, U/L | 17 (12–24) | 28 (20–39) |
| AST, U/L | 20 (17–24) | 24 (20–28) |
| TC, mmol/L | 4.74 (4.13–5.35) | 5.08 (4.53–5.61) |
| TG, mmol/L | 1.05 (0.80–1.47) | 1.875 (1.35–2.585) |
| LDL-c, mmol/L | 2.75 (2.23–3.24) | 2.95 (2.41–3.48) |
| HDL-c mmol/L | 1.44 (1.17–1.71) | 1.13 (1.00–1.29) |
| HbA1c, % | 5.3 (5.1–5.6) | 5.6 (5.3–6.0) |
| TMAVA, μ M | 0.593 (0.448–0.771) | 0.627 (0.466, 0.826) ^a |
| TML, μ M | 1.04 (0.7935–1.39) | 1.14 (0.933–1.41) ^a |
| γ -BB, μ M | 1.15 (0.962–1.38) | 1.26 (1.06–1.42) ^a |
| Carnitine, μ M | 61.89 (53.21–70.085) | 66.3 (57.9–73.61) ^a |

NOTE. Data were expressed as mean \pm SD for normal distribution and as median (interquartile range, 25%–75%) for skewed variables.

ALT, alanine transaminase; AST, alanine transaminase; HbA1c, hemoglobin A1c; LDL-c, low density lipoprotein cholesterol; HDL-c, high-density lipoprotein cholesterol; TC, total cholesterol; TG, triglycerides.

^a $P < .05$.

Supplementary Table 5. Odds Ratio for Patients With Liver Steatosis in the Top Quartile of Metabolite Compared With Patients in the Lowest Quartile

| Variable | Fatty liver (n = 273) | Healthy (n = 494) | OR | 95% CI | P value |
|-----------------------|--------------------------|----------------------|------|-----------|---------|
| TMAVA, μ M | 0.593 (0.45–0.77) | 0.627 (0.47–0.83) | 1.82 | 1.14–2.90 | .012 |
| TML, μ M | 1.04 (0.79–1.39) | 1.14 (0.93–1.41) | 1.33 | 1.02–1.73 | .033 |
| γ -BB, μ M | 1.15 (0.96–1.38) | 1.26 (1.06–1.42) | 2.02 | 1.25–3.27 | .004 |
| Carnitine, μ M | 61.89 (53.21–70.09) | 66.3 (57.90–73.61) | 1.03 | 1.02–1.04 | .000 |

NOTE. Data were expressed as median (interquartile range, 25%–75%).

OR, odds ratio.

Supplementary Table 6. Plasma Samples Were Spiked With Internal Standards and the Accuracy of TMAVA Concentration Was Calculated

| Standard concentrations, μM | Accuracy, % |
|----------------------------------|-------------|
| 0.0975 | 91.8 |
| 0.195 | 93.2 |
| 0.39 | 102 |
| 0.78 | 102 |
| 1.56 | 105 |
| 3.125 | 103 |
| 6.25 | 105 |
| 12.5 | 101 |
| 25 | 97.4 |

| Quality control ^a | Mean \pm SD, μM | CV% |
|------------------------------|------------------------|------|
| 1 | 0.70 \pm 0.01 | 2.09 |
| 2 | 0.92 \pm 0.02 | 2.27 |
| 3 | 7.09 \pm 0.12 | 1.68 |

NOTE. The calculated mean, SD, CV% are given and the CV % values are <10%.

^aThree quality control samples with different TMAVA concentrations were measured every 20 samples.

Supplementary Table 7. Biological Processes Analysis of the Liver Proteomics

| Term | n | % | P value | Benjamini |
|--|----|------|----------|-----------|
| Oxidation-reduction process | 97 | 22 | 5.90E-50 | 1.10E-46 |
| Metabolic process | 54 | 12.2 | 7.90E-23 | 7.30E-20 |
| Lipid metabolic process | 50 | 11.3 | 7.30E-20 | 4.50E-17 |
| Fatty acid metabolic process | 31 | 7 | 1.00E-19 | 4.90E-17 |
| Fatty acid β -oxidation | 15 | 3.4 | 4.30E-13 | 1.60E-10 |
| Liver development | 17 | 3.9 | 3.50E-10 | 1.10E-07 |
| Protein folding | 19 | 4.3 | 6.00E-10 | 1.60E-07 |
| Steroid metabolic process | 15 | 3.4 | 5.20E-09 | 1.20E-06 |
| ATP biosynthetic process | 9 | 2 | 2.20E-08 | 4.60E-06 |
| ATP metabolic process | 10 | 2.3 | 2.00E-07 | 3.70E-05 |
| Carbohydrate metabolic process | 20 | 4.5 | 2.20E-07 | 3.70E-05 |
| Nitrogen compound metabolic process | 8 | 1.8 | 3.50E-07 | 5.50E-05 |
| Cell redox homeostasis | 11 | 2.5 | 1.80E-06 | 2.50E-04 |
| Drug metabolic process | 7 | 1.6 | 1.90E-06 | 2.40E-04 |
| Fatty acid β -oxidation using acyl-CoA dehydrogenase | 7 | 1.6 | 2.70E-06 | 3.30E-04 |
| Response to drug | 24 | 5.4 | 2.90E-06 | 3.30E-04 |
| Acyl-CoA metabolic process | 8 | 1.8 | 4.60E-06 | 5.00E-04 |
| ATP synthesis coupled proton transport | 7 | 1.6 | 9.10E-06 | 9.40E-04 |
| Oxaloacetate metabolic process | 6 | 1.4 | 9.50E-06 | 9.30E-04 |
| Steroid biosynthetic process | 10 | 2.3 | 9.60E-06 | 8.90E-04 |
| Translation | 25 | 5.7 | 1.50E-05 | 1.30E-03 |
| Cell-cell adhesion | 16 | 3.6 | 2.60E-05 | 2.20E-03 |
| Cholesterol metabolic process | 11 | 2.5 | 3.10E-05 | 2.50E-03 |
| Lipid homeostasis | 8 | 1.8 | 3.20E-05 | 2.50E-03 |
| Tricarboxylic acid cycle | 7 | 1.6 | 3.80E-05 | 2.80E-03 |
| NADH metabolic process | 5 | 1.1 | 1.10E-04 | 7.70E-03 |
| Translational initiation | 8 | 1.8 | 2.00E-04 | 1.30E-02 |
| Response to aluminum ion | 4 | 0.9 | 2.20E-04 | 1.40E-02 |
| Cellular response to interleukin-4 | 6 | 1.4 | 3.00E-04 | 1.90E-02 |
| Sterol biosynthetic process | 6 | 1.4 | 3.00E-04 | 1.90E-02 |
| Response to endoplasmic reticulum stress | 9 | 2 | 3.00E-04 | 1.90E-02 |
| Response to ethanol | 11 | 2.5 | 3.10E-04 | 1.90E-02 |
| Acetyl-CoA metabolic process | 4 | 0.9 | 3.70E-04 | 2.10E-02 |
| Response to cadmium ion | 6 | 1.4 | 4.30E-04 | 2.40E-02 |
| Cholesterol biosynthetic process | 6 | 1.4 | 6.90E-04 | 3.70E-02 |
| Glutathione metabolic process | 7 | 1.6 | 7.70E-04 | 4.00E-02 |
| Carnitine metabolic process | 4 | 0.9 | 8.60E-04 | 4.30E-02 |
| Response to oxidative stress | 11 | 2.5 | 8.60E-04 | 4.20E-02 |
| Response to zinc ion | 6 | 1.4 | 1.00E-03 | 5.00E-02 |
| Ribosomal small subunit assembly | 5 | 1.1 | 1.10E-03 | 5.20E-02 |
| Response to selenium ion | 4 | 0.9 | 1.20E-03 | 5.40E-02 |
| Fatty acid catabolic process | 4 | 0.9 | 1.20E-03 | 5.40E-02 |
| Protein homotetramerization | 8 | 1.8 | 1.40E-03 | 6.00E-02 |
| Carnitine metabolic process | 3 | 0.7 | 1.50E-03 | 6.40E-02 |
| Urea cycle | 4 | 0.9 | 1.60E-03 | 6.80E-02 |
| Actin filament network formation | 4 | 0.9 | 1.60E-03 | 6.80E-02 |
| Response to cold | 6 | 1.4 | 1.90E-03 | 7.80E-02 |
| Cellular response to testosterone stimulus | 4 | 0.9 | 2.10E-03 | 8.40E-02 |
| Mitochondrion organization | 8 | 1.8 | 2.30E-03 | 8.90E-02 |
| Gluconeogenesis | 5 | 1.1 | 2.60E-03 | 9.60E-02 |
| Carnitine biosynthetic process | 3 | 0.7 | 2.90E-03 | 1.10E-01 |
| Detoxification of copper ion | 3 | 0.7 | 2.90E-03 | 1.10E-01 |
| Xanthine catabolic process | 3 | 0.7 | 4.80E-03 | 1.70E-01 |
| Cellular response to glucagon stimulus | 3 | 0.7 | 4.80E-03 | 1.70E-01 |
| Acetyl-CoA biosynthetic process | 3 | 0.7 | 4.80E-03 | 1.70E-01 |
| Ribosomal subunit export from nucleus | 3 | 0.7 | 4.80E-03 | 1.70E-01 |
| Cellular response to cAMP | 6 | 1.4 | 5.20E-03 | 1.80E-01 |
| Aging | 11 | 2.5 | 5.90E-03 | 1.90E-01 |
| Fatty acid biosynthetic process | 7 | 1.6 | 6.40E-03 | 2.00E-01 |
| Transport | 58 | 13.2 | 6.70E-03 | 2.10E-01 |
| Brown fat cell differentiation | 5 | 1.1 | 6.90E-03 | 2.10E-01 |

Supplementary Table 7. Continued

| Term | n | % | P value | Benjamini |
|---|----|-----|----------|-----------|
| Ribosomal small subunit export from nucleus | 3 | 0.7 | 7.10E-03 | 2.10E-01 |
| Apoptotic cell clearance | 4 | 0.9 | 7.20E-03 | 2.10E-01 |
| Long-chain fatty acid metabolic process | 4 | 0.9 | 7.20E-03 | 2.10E-01 |
| Toxin transport | 5 | 1.1 | 7.60E-03 | 2.20E-01 |
| Heme biosynthetic process | 4 | 0.9 | 8.40E-03 | 2.40E-01 |
| Organ regeneration | 6 | 1.4 | 8.40E-03 | 2.30E-01 |
| Glutamine metabolic process | 4 | 0.9 | 9.70E-03 | 2.60E-01 |
| Peroxisome organization | 4 | 0.9 | 9.70E-03 | 2.60E-01 |
| Proton transport | 6 | 1.4 | 9.70E-03 | 2.60E-01 |
| Very long-chain fatty acid catabolic process | 3 | 0.7 | 9.80E-03 | 2.60E-01 |
| Fatty acid elongation | 3 | 0.7 | 9.80E-03 | 2.60E-01 |
| Arginine biosynthetic process | 3 | 0.7 | 9.80E-03 | 2.60E-01 |
| Response to methylmercury | 3 | 0.7 | 9.80E-03 | 2.60E-01 |
| Response to starvation | 5 | 1.1 | 1.00E-02 | 2.60E-01 |
| Glucose homeostasis | 4 | 0.9 | 1.10E-02 | 2.70E-01 |
| Response to reactive oxygen species | 4 | 0.9 | 1.10E-02 | 2.70E-01 |
| Positive regulation of glucose metabolic process | 5 | 1.1 | 1.10E-02 | 2.70E-01 |
| Triglyceride metabolic process | 9 | 2 | 1.10E-02 | 2.60E-01 |
| Internal protein amino acid acetylation | 3 | 0.7 | 1.30E-02 | 3.00E-01 |
| Positive regulation of cholesterol biosynthetic process | 3 | 0.7 | 1.30E-02 | 3.00E-01 |
| Mitochondrial acetyl-CoA biosynthetic Process from pyruvate | 3 | 0.7 | 1.30E-02 | 3.00E-01 |
| Glycerol-3-phosphate metabolic process | 3 | 0.7 | 1.30E-02 | 3.00E-01 |
| Positive regulation of protein localization to Cajal body | 3 | 0.7 | 1.30E-02 | 3.00E-01 |
| Regulation of the force of heart contraction | 4 | 0.9 | 1.40E-02 | 3.30E-01 |
| Iron ion homeostasis | 5 | 1.1 | 1.40E-02 | 3.20E-01 |
| Cellular amino acid metabolic process | 4 | 0.9 | 1.60E-02 | 3.50E-01 |
| Xenobiotic metabolic process | 4 | 0.9 | 1.60E-02 | 3.50E-01 |
| Glycine metabolic process | 3 | 0.7 | 1.60E-02 | 3.50E-01 |
| Regulation of cholesterol metabolic process | 3 | 0.7 | 1.60E-02 | 3.50E-01 |
| Response to amine | 3 | 0.7 | 1.60E-02 | 3.50E-01 |
| Protein refolding | 3 | 0.7 | 1.60E-02 | 3.50E-01 |
| Positive regulation of nitric oxide biosynthetic process | 5 | 1.1 | 1.80E-02 | 3.80E-01 |
| Lactation | 3 | 0.7 | 2.00E-02 | 4.00E-01 |
| Protein deglycosylation | 3 | 0.7 | 2.00E-02 | 4.00E-01 |
| Protein import into peroxisome matrix | 5 | 1.1 | 2.00E-02 | 3.90E-01 |
| Response to insulin | 6 | 1.4 | 2.20E-02 | 4.20E-01 |
| Response to immobilization stress | 4 | 0.9 | 2.20E-02 | 4.20E-01 |
| Response to activity | 5 | 1.1 | 2.40E-02 | 4.40E-01 |
| Bile acid biosynthetic process | 3 | 0.7 | 2.40E-02 | 4.40E-01 |
| Negative regulation of oxidative stress-induced intrinsic apoptotic signaling pathway | 3 | 0.7 | 2.40E-02 | 4.40E-01 |
| Erythrocyte homeostasis | 3 | 0.7 | 2.40E-02 | 4.40E-01 |
| Negative regulation of neuron apoptotic process | 9 | 2 | 2.90E-02 | 4.90E-01 |
| Tetrahydrofolate interconversion | 3 | 0.7 | 2.90E-02 | 4.90E-01 |
| Actin crosslink formation | 3 | 0.7 | 2.90E-02 | 4.90E-01 |
| Epoxygenase P450 pathway | 4 | 0.9 | 2.90E-02 | 4.90E-01 |
| One-carbon metabolic process | 4 | 0.9 | 3.20E-02 | 5.20E-01 |
| Chaperone mediated protein folding requiring cofactor | 3 | 0.7 | 3.30E-02 | 5.30E-01 |
| Positive regulation of podosome assembly | 3 | 0.7 | 3.30E-02 | 5.30E-01 |
| Porphyrin-containing compound biosynthetic process | 3 | 0.7 | 3.30E-02 | 5.30E-01 |
| Mitochondrion morphogenesis | 4 | 0.9 | 3.50E-02 | 5.40E-01 |
| Chaperone-mediated protein folding | 4 | 0.9 | 3.50E-02 | 5.40E-01 |
| Regulation of translational initiation | 4 | 0.9 | 3.80E-02 | 5.70E-01 |
| Positive regulation of gene expression | 3 | 0.7 | 3.80E-02 | 5.70E-01 |
| Lipid biosynthetic process | 3 | 0.7 | 3.80E-02 | 5.70E-01 |
| Androgen metabolic process | 16 | 3.6 | 3.80E-02 | 5.60E-01 |
| Positive regulation of translation | 5 | 1.1 | 3.90E-02 | 5.70E-01 |
| Response to heat | 5 | 1.1 | 3.90E-02 | 5.70E-01 |
| Response to hydrogen peroxide | 5 | 1.1 | 4.10E-02 | 5.90E-01 |
| Osteoblast differentiation | 7 | 1.6 | 4.30E-02 | 5.90E-01 |
| Positive regulation of telomerase RNA localization to Cajal body | 3 | 0.7 | 4.40E-02 | 6.00E-01 |
| Nitric oxide mediated signal transduction | 3 | 0.7 | 4.40E-02 | 6.00E-01 |

Supplementary Table 7. Continued

| Term | n | % | P value | Benjamini |
|--|---|-----|----------|-----------|
| Heat generation | 3 | 0.7 | 4.40E-02 | 6.00E-01 |
| Positive regulation of lipid metabolic process | 3 | 0.7 | 4.40E-02 | 6.00E-01 |
| Cellular response to lipid | 3 | 0.7 | 4.40E-02 | 6.00E-01 |
| Positive regulation of transcription from RNA polymerase II promoter in response to acidic pH | 2 | 0.5 | 4.50E-02 | 6.00E-01 |
| Phytol metabolic process | 2 | 0.5 | 4.50E-02 | 6.00E-01 |
| Negative regulation of nitrosative stress-induced intrinsic apoptotic signaling pathway | 2 | 0.5 | 4.50E-02 | 6.00E-01 |
| Methylglyoxal metabolic process | 2 | 0.5 | 4.50E-02 | 6.00E-01 |
| Monoterpenoid metabolic process | 2 | 0.5 | 4.50E-02 | 6.00E-01 |
| Acetyl-CoA catabolic process | 2 | 0.5 | 4.50E-02 | 6.00E-01 |
| Response to toxic substance | 6 | 1.4 | 4.50E-02 | 6.00E-01 |
| Receptor-mediated endocytosis | 5 | 1.1 | 4.60E-02 | 6.00E-01 |
| Binding of sperm to zona pellucida | 4 | 0.9 | 4.70E-02 | 6.10E-01 |
| Cellular response to insulin stimulus | 6 | 1.4 | 4.80E-02 | 6.20E-01 |
| Negative regulation of lipid biosynthetic process | 3 | 0.7 | 4.90E-02 | 6.20E-01 |
| Very long-chain fatty acid metabolic process | 3 | 0.7 | 4.90E-02 | 6.20E-01 |
| Response to lead ion | 3 | 0.7 | 4.90E-02 | 6.20E-01 |
| Homeostasis of number of cells within a tissue | 4 | 0.9 | 5.30E-02 | 6.50E-01 |
| Platelet aggregation | 4 | 0.9 | 5.30E-02 | 6.50E-01 |
| Fatty acid oxidation | 3 | 0.7 | 5.50E-02 | 6.50E-01 |
| Isoprenoid biosynthetic process | 3 | 0.7 | 5.50E-02 | 6.50E-01 |
| Aerobic respiration | 4 | 0.9 | 5.70E-02 | 6.60E-01 |
| Actin filament capping | 3 | 0.7 | 6.10E-02 | 6.80E-01 |
| Carboxylic acid metabolic process | 3 | 0.7 | 6.10E-02 | 6.80E-01 |
| Fatty acid transport | 3 | 0.7 | 6.10E-02 | 6.80E-01 |
| Protein tetramerization | 4 | 0.9 | 6.40E-02 | 7.00E-01 |
| Positive regulation of superoxide dismutase activity | 2 | 0.5 | 6.60E-02 | 7.10E-01 |
| Vitamin K metabolic process | 2 | 0.5 | 6.60E-02 | 7.10E-01 |
| Medium-chain fatty acid metabolic process | 2 | 0.5 | 6.60E-02 | 7.10E-01 |
| Peroxisome membrane biogenesis | 2 | 0.5 | 6.60E-02 | 7.10E-01 |
| Vacuolar protein processing | 2 | 0.5 | 6.60E-02 | 7.10E-01 |
| Organic acid metabolic process | 2 | 0.5 | 6.60E-02 | 7.10E-01 |
| Heterocycle metabolic process | 2 | 0.5 | 6.60E-02 | 7.10E-01 |
| Regulation of protein catabolic process | 3 | 0.7 | 6.70E-02 | 7.10E-01 |
| Ribosomal small subunit biogenesis | 3 | 0.7 | 6.70E-02 | 7.10E-01 |
| Response to fatty acid | 3 | 0.7 | 6.70E-02 | 7.10E-01 |
| Negative regulation of lipid storage | 3 | 0.7 | 6.70E-02 | 7.10E-01 |
| Response to lipopolysaccharide | 9 | 2 | 7.80E-02 | 7.60E-01 |
| Temperature homeostasis | 3 | 0.7 | 8.00E-02 | 7.70E-01 |
| Negative regulation of insulin secretion involved in cellular response to glucose stimulus | 3 | 0.7 | 8.70E-02 | 7.90E-01 |
| Energy reserve metabolic process | 3 | 0.7 | 8.70E-02 | 7.90E-01 |
| L-ascorbic acid biosynthetic process | 2 | 0.5 | 8.70E-02 | 7.90E-01 |
| Histidine catabolic process | 2 | 0.5 | 8.70E-02 | 7.90E-01 |
| Arginine metabolic process | 2 | 0.5 | 8.70E-02 | 7.90E-01 |
| Negative regulation of oxidative stress-induced cell death | 2 | 0.5 | 8.70E-02 | 7.90E-01 |
| Angiotensin mediated vasoconstriction involved in regulation of systemic arterial blood pressure | 2 | 0.5 | 8.70E-02 | 7.90E-01 |
| Positive regulation by host of viral release from host cell | 2 | 0.5 | 8.70E-02 | 7.90E-01 |
| Positive regulation of oxidative stress-induced intrinsic apoptotic signaling pathway | 2 | 0.5 | 8.70E-02 | 7.90E-01 |
| CoA metabolic process | 2 | 0.5 | 8.70E-02 | 7.90E-01 |
| dATP metabolic process | 2 | 0.5 | 8.70E-02 | 7.90E-01 |
| Positive regulation by virus of viral protein levels in host cell | 2 | 0.5 | 8.70E-02 | 7.90E-01 |
| Histidine catabolic process to glutamate and formamide | 2 | 0.5 | 8.70E-02 | 7.90E-01 |
| Negative regulation of transcription factor import into nucleus | 2 | 0.5 | 8.70E-02 | 7.90E-01 |
| Response to insecticide | 2 | 0.5 | 8.70E-02 | 7.90E-01 |
| Triglyceride transport | 2 | 0.5 | 8.70E-02 | 7.90E-01 |
| ADP biosynthetic process | 2 | 0.5 | 8.70E-02 | 7.90E-01 |
| Cellular response to potassium ion starvation | 2 | 0.5 | 8.70E-02 | 7.90E-01 |
| Response to fructose | 2 | 0.5 | 8.70E-02 | 7.90E-01 |
| Citrulline metabolic process | 2 | 0.5 | 8.70E-02 | 7.90E-01 |
| Mitochondrial ATP synthesis coupled proton transport | 2 | 0.5 | 8.70E-02 | 7.90E-01 |
| Histidine catabolic process to glutamate and formate | 2 | 0.5 | 8.70E-02 | 7.90E-01 |
| Positive regulation of protein localization to early endosome | 2 | 0.5 | 8.70E-02 | 7.90E-01 |

Supplementary Table 7. Continued

| Term | n | % | P value | Benjamini |
|--|----|-----|----------|-----------|
| Regulation of organelle assembly | 2 | 0.5 | 8.70E-02 | 7.90E-01 |
| Protein catabolic process | 4 | 0.9 | 8.90E-02 | 7.90E-01 |
| Negative regulation of apoptotic process | 19 | 4.3 | 9.00E-02 | 7.90E-01 |
| Response to hormone | 4 | 0.9 | 9.30E-02 | 8.00E-01 |
| Erythrocyte differentiation | 4 | 0.9 | 9.30E-02 | 8.00E-01 |
| Response to organonitrogen compound | 3 | 0.7 | 9.40E-02 | 8.00E-01 |
| ER to Golgi vesicle-mediated transport | 5 | 1.1 | 9.90E-02 | 8.20E-01 |

ADP, adenosine diphosphate; ATP, adenosine triphosphate; cAMP, adenosine 3',5'-cyclic monophosphate; CoA, coenzyme A; dATP, deoxyadenosine triphosphate; ER, endoplasmic reticulum; NADH, reduced nicotinamide adenine dinucleotide.

Supplementary Table 8. Cellular Component Analysis of the Liver Proteomics

| Term | n | % | P value | Benjamini |
|---|-----|------|----------|-----------|
| Mitochondrion | 170 | 38.5 | 5.40E-69 | 1.90E-66 |
| Extracellular exosome | 202 | 45.8 | 3.50E-64 | 6.10E-62 |
| Mitochondrial inner membrane | 61 | 13.8 | 9.00E-34 | 1.10E-31 |
| Myelin sheath | 34 | 7.7 | 2.20E-20 | 1.90E-18 |
| Mitochondrial matrix | 32 | 7.3 | 1.10E-18 | 7.90E-17 |
| Cytosol | 97 | 22 | 2.50E-17 | 1.50E-15 |
| Endoplasmic reticulum | 79 | 17.9 | 4.40E-16 | 2.20E-14 |
| Peroxisome | 25 | 5.7 | 9.20E-16 | 3.90E-14 |
| Cytoplasm | 221 | 50.1 | 2.20E-14 | 8.50E-13 |
| Intracellular membrane-bounded organelle | 53 | 12 | 1.50E-13 | 5.40E-12 |
| Organelle membrane | 19 | 4.3 | 1.70E-12 | 5.40E-11 |
| Extracellular matrix | 31 | 7 | 2.40E-12 | 7.00E-11 |
| Cell-cell adherens junction | 29 | 6.6 | 3.60E-10 | 9.80E-09 |
| Focal adhesion | 32 | 7.3 | 6.40E-10 | 1.60E-08 |
| Melanosome | 15 | 3.4 | 4.00E-08 | 9.40E-07 |
| Endoplasmic reticulum membrane | 41 | 9.3 | 4.30E-08 | 9.50E-07 |
| Endoplasmic reticulum chaperone complex | 7 | 1.6 | 8.50E-08 | 1.80E-06 |
| Endoplasmic reticulum lumen | 13 | 2.9 | 2.80E-06 | 5.40E-05 |
| Mitochondrial nucleoid | 9 | 2 | 6.00E-06 | 1.10E-04 |
| Intracellular ribonucleoprotein complex | 22 | 5 | 7.90E-06 | 1.40E-04 |
| Membrane | 195 | 44.2 | 1.70E-05 | 2.90E-04 |
| Peroxisomal membrane | 9 | 2 | 1.80E-05 | 2.80E-04 |
| Mitochondrial proton-transporting ATP synthase complex | 6 | 1.4 | 3.20E-05 | 5.00E-04 |
| Respiratory chain | 9 | 2 | 3.50E-05 | 5.10E-04 |
| Mitochondrial respiratory chain complex I | 8 | 1.8 | 6.50E-05 | 9.20E-04 |
| Mitochondrial membrane | 11 | 2.5 | 7.10E-05 | 9.60E-04 |
| Blood microparticle | 12 | 2.7 | 1.60E-04 | 2.10E-03 |
| Integral component of endoplasmic reticulum membrane | 10 | 2.3 | 2.10E-04 | 2.60E-03 |
| Smooth endoplasmic reticulum | 6 | 1.4 | 3.70E-04 | 4.50E-03 |
| Cortical cytoskeleton | 6 | 1.4 | 5.10E-04 | 6.00E-03 |
| Proteasome complex | 8 | 1.8 | 5.70E-04 | 6.40E-03 |
| Podosome | 6 | 1.4 | 5.90E-04 | 6.50E-03 |
| Extracellular space | 52 | 11.8 | 1.10E-03 | 1.10E-02 |
| Cell body | 9 | 2 | 1.70E-03 | 1.80E-02 |
| Zona pellucida receptor complex | 4 | 0.9 | 2.50E-03 | 2.50E-02 |
| Mitochondrial proton-transporting ATP synthase complex, catalytic core F(1) | 3 | 0.7 | 4.50E-03 | 4.40E-02 |
| Proton-transporting ATP synthase complex, catalytic core F(1) | 3 | 0.7 | 4.50E-03 | 4.40E-02 |
| Nucleoplasm | 60 | 13.6 | 5.00E-03 | 4.70E-02 |
| Peroxisomal matrix | 4 | 0.9 | 5.50E-03 | 5.00E-02 |
| Cytosolic small ribosomal subunit | 6 | 1.4 | 5.80E-03 | 5.10E-02 |
| Mitochondrial intermembrane space | 7 | 1.6 | 5.80E-03 | 5.00E-02 |
| Mitochondrial outer membrane | 10 | 2.3 | 6.40E-03 | 5.40E-02 |
| Mitochondrial envelope | 4 | 0.9 | 7.70E-03 | 6.30E-02 |
| Cell | 12 | 2.7 | 1.30E-02 | 1.00E-01 |

Supplementary Table 8. Continued

| Term | n | % | P value | Benjamini |
|--|----|-----|----------|-----------|
| Lipid particle | 6 | 1.4 | 1.40E-02 | 1.10E-01 |
| Chaperonin-containing T-complex | 3 | 0.7 | 1.50E-02 | 1.10E-01 |
| Protein complex | 23 | 5.2 | 2.00E-02 | 1.40E-01 |
| Ribosome | 10 | 2.3 | 2.20E-02 | 1.60E-01 |
| Cytoplasmic ribonucleoprotein granule | 4 | 0.9 | 2.20E-02 | 1.50E-01 |
| Mitochondrial crista | 3 | 0.7 | 2.30E-02 | 1.50E-01 |
| Midbody | 8 | 1.8 | 2.40E-02 | 1.60E-01 |
| Proton-transporting ATP synthase complex, coupling factor F(o) | 3 | 0.7 | 2.70E-02 | 1.70E-01 |
| Mitochondrial proton-transporting ATP synthase complex, coupling factor F(o) | 3 | 0.7 | 2.70E-02 | 1.70E-01 |
| Fascia adherens | 3 | 0.7 | 3.10E-02 | 2.00E-01 |
| Proteasome regulatory particle, base subcomplex | 3 | 0.7 | 3.10E-02 | 2.00E-01 |
| COP9 signalosome | 4 | 0.9 | 3.40E-02 | 2.10E-01 |
| Integral component of peroxisomal membrane | 3 | 0.7 | 3.60E-02 | 2.10E-01 |
| Apical part of cell | 7 | 1.6 | 4.00E-02 | 2.30E-01 |
| Intermediate filament | 7 | 1.6 | 4.30E-02 | 2.40E-01 |
| Succinate-CoA ligase complex (GDP-forming) | 2 | 0.5 | 4.30E-02 | 2.40E-01 |
| Mitochondrial fatty acid beta-oxidation multienzyme complex | 2 | 0.5 | 4.30E-02 | 2.40E-01 |
| Proteasome accessory complex | 3 | 0.7 | 5.20E-02 | 2.80E-01 |
| Stress fiber | 5 | 1.1 | 5.80E-02 | 3.00E-01 |
| Lysosome | 13 | 2.9 | 5.90E-02 | 3.00E-01 |
| Nuclear matrix | 6 | 1.4 | 6.10E-02 | 3.00E-01 |
| Endoplasmic reticulum-Golgi intermediate compartment | 5 | 1.1 | 6.10E-02 | 3.00E-01 |
| Inclusion body | 3 | 0.7 | 6.30E-02 | 3.10E-01 |
| Rough endoplasmic reticulum | 5 | 1.1 | 6.30E-02 | 3.00E-01 |
| Glycerol-3-phosphate dehydrogenase complex | 2 | 0.5 | 6.40E-02 | 3.00E-01 |
| Perinuclear region of cytoplasm | 22 | 5 | 8.00E-02 | 3.60E-01 |
| Viral nucleocapsid | 3 | 0.7 | 8.20E-02 | 3.60E-01 |
| Extracellular vesicle | 4 | 0.9 | 9.10E-02 | 3.90E-01 |
| Ruffle membrane | 5 | 1.1 | 9.40E-02 | 4.00E-01 |

ATP, adenosine triphosphate; CoA, coenzyme A; GDP, guanosine diphosphate.

Supplementary Table 9. Protein Functional Clustering of the Liver Proteomics

| Annotation of the functional clustering | | n | P value | Benjamini |
|--|--|-----|----------|-----------|
| Annotation Cluster 1: Enrichment Score: 45.5 | Oxidation-reduction process | 97 | 5.90E-50 | 1.10E-46 |
| | Oxidoreductase | 88 | 2.60E-48 | 4.00E-46 |
| | Oxidoreductase activity | 85 | 2.10E-40 | 1.60E-37 |
| Annotation Cluster 2: Enrichment Score: 33.17 | Mitochondrion | 102 | 4.80E-42 | 4.90E-40 |
| | Mitochondrial inner membrane | 61 | 9.00E-34 | 1.10E-31 |
| | Transit peptide | 65 | 3.00E-33 | 2.30E-31 |
| | Transit peptide: Mitochondrion | 61 | 1.60E-26 | 1.70E-23 |
| Annotation Cluster 3: Enrichment Score: 16.02 | Lipid metabolism | 45 | 4.70E-20 | 2.40E-18 |
| | Lipid metabolic process | 50 | 7.30E-20 | 4.50E-17 |
| | Fatty acid metabolic process | 31 | 1.00E-19 | 4.90E-17 |
| | Fatty acid metabolism | 25 | 1.80E-17 | 6.70E-16 |
| | Fatty acid beta-oxidation | 15 | 4.30E-13 | 1.60E-10 |
| | Fatty acid metabolism | 16 | 2.90E-10 | 8.00E-09 |
| Annotation Cluster 4: Enrichment Score: 13.13 | Endoplasmic reticulum | 65 | 2.20E-17 | 7.40E-16 |
| | Endoplasmic reticulum | 79 | 4.40E-16 | 2.20E-14 |
| | Endoplasmic reticulum membrane | 41 | 4.30E-08 | 9.50E-07 |
| Annotation Cluster 5: Enrichment Score: 10.56 | Peroxisome | 23 | 1.00E-16 | 3.30E-15 |
| | Peroxisome | 25 | 9.20E-16 | 3.90E-14 |
| | Peroxisome | 21 | 1.70E-11 | 5.30E-10 |
| | Short sequence motif: microbody targeting signal | 11 | 5.90E-08 | 7.70E-06 |
| | Receptor binding | 24 | 1.80E-04 | 4.60E-03 |
| Annotation Cluster 6: Enrichment Score: 9.14 | Chaperone | 23 | 2.40E-11 | 4.10E-10 |
| | Protein folding | 19 | 6.00E-10 | 1.60E-07 |
| | Unfolded protein binding | 14 | 2.50E-08 | 1.60E-06 |
| Annotation Cluster 7: Enrichment Score: 7.91 | Cadherin binding involved in cell-cell adhesion | 29 | 2.00E-10 | 3.10E-08 |
| | Cell-cell adherens junction | 29 | 3.60E-10 | 9.80E-09 |
| | Cell-cell adhesion | 16 | 2.60E-05 | 2.20E-03 |

Supplementary Table 9. Continued

| Annotation of the functional clustering | | n | P value | Benjamini | |
|---|---|--|----------|-----------|----------|
| Annotation Cluster 8: Enrichment Score: 7.09 | Nucleotide-binding | 73 | 1.00E-09 | 1.50E-08 | |
| | ATP-binding | 59 | 1.50E-08 | 2.00E-07 | |
| | Nucleotide binding | 81 | 9.30E-07 | 3.80E-05 | |
| | ATP binding | 66 | 2.90E-06 | 9.40E-05 | |
| Annotation Cluster 9: Enrichment Score: 6.75 | FAD | 21 | 1.30E-13 | 2.70E-12 | |
| | Flavoprotein | 21 | 8.80E-13 | 1.70E-11 | |
| | Nucleotide phosphate-binding region: FAD | 15 | 4.90E-11 | 1.70E-08 | |
| | Flavin adenine dinucleotide binding | 16 | 1.40E-10 | 2.70E-08 | |
| | Electron carrier activity | 14 | 2.70E-10 | 3.50E-08 | |
| | Binding site: substrate; via amide nitrogen | 11 | 1.10E-09 | 2.30E-07 | |
| | Fatty-acyl-CoA binding | 11 | 6.40E-09 | 6.20E-07 | |
| | Oxidoreductase activity, acting on the CH-CH group of donors | 9 | 2.20E-07 | 9.90E-06 | |
| | Acyl-CoA dehydrogenase/oxidase, N-terminal | 7 | 2.20E-07 | 2.50E-05 | |
| | Acyl-CoA dehydrogenase, conserved site | 6 | 4.80E-07 | 4.40E-05 | |
| | Acyl-CoA oxidase/dehydrogenase, central domain | 7 | 5.70E-07 | 4.80E-05 | |
| | Acyl-CoA dehydrogenase/oxidase | 7 | 5.70E-07 | 4.80E-05 | |
| | Acyl-CoA dehydrogenase/oxidase C-terminal | 7 | 5.70E-07 | 4.80E-05 | |
| | Binding site: FAD | 8 | 5.80E-07 | 6.80E-05 | |
| | Acyl-CoA dehydrogenase activity | 7 | 1.90E-06 | 6.90E-05 | |
| | Fatty acid beta-oxidation using acyl-CoA dehydrogenase | 7 | 2.70E-06 | 3.30E-04 | |
| | Oxidoreductase activity, acting on the CH-CH group of donors, with a flavin as acceptor | 6 | 2.80E-05 | 8.30E-04 | |
| | Lipid homeostasis | 8 | 3.20E-05 | 2.50E-03 | |
| | Binding site: Substrate; via carbonyl oxygen | 7 | 3.50E-05 | 3.40E-03 | |
| | Long-chain-acyl-CoA dehydrogenase activity | 3 | 1.70E-03 | 3.60E-02 | |
| | Binding site: FAD; shared with dimeric partner | 3 | 5.10E-03 | 1.90E-01 | |
| | Nucleotide phosphate-binding region: FAD; shared with dimeric partner | 3 | 5.10E-03 | 1.90E-01 | |
| | Annotation Cluster 10: Enrichment Score: 6.32 | Microsome | 24 | 1.00E-15 | 2.50E-14 |
| | | Iron | 37 | 3.10E-15 | 7.30E-14 |
| | | Intracellular membrane-bounded organelle | 53 | 1.50E-13 | 5.40E-12 |
| | | Organelle membrane | 19 | 1.70E-12 | 5.40E-11 |
| | | Iron ion binding | 25 | 3.50E-10 | 3.80E-08 |
| Heme | | 20 | 1.00E-09 | 1.50E-08 | |
| Monooxygenase activity | | 17 | 6.70E-09 | 5.70E-07 | |
| Monooxygenase | | 17 | 6.90E-09 | 9.50E-08 | |
| Heme binding | | 21 | 8.90E-09 | 6.90E-07 | |
| Cytochrome P450, conserved site | | 15 | 1.40E-08 | 3.50E-06 | |
| Cytochrome P450, E-class, group I | | 14 | 1.90E-08 | 3.90E-06 | |
| Cytochrome P450 | | 15 | 4.00E-08 | 6.70E-06 | |
| Metal ion-binding site: Iron (heme axial ligand) | | 16 | 5.50E-08 | 8.30E-06 | |
| Oxidoreductase activity, acting on paired donors, with incorporation or reduction of molecular oxygen | | 15 | 1.10E-07 | 5.20E-06 | |
| Retinol metabolism | | 14 | 2.50E-05 | 3.50E-04 | |
| Secondary metabolites biosynthesis, transport, and catabolism | | 16 | 4.20E-05 | 4.00E-04 | |
| Aromatase activity | | 7 | 2.00E-04 | 5.00E-03 | |
| Oxidoreductase activity, acting on paired donors, with incorporation or reduction of molecular oxygen, reduced flavin or flavoprotein as one donor, and incorporation of one atom of oxygen | | 7 | 4.80E-04 | 1.10E-02 | |
| Arachidonic acid epoxygenase activity | | 7 | 8.90E-04 | 2.00E-02 | |
| Steroid hormone biosynthesis | | 11 | 1.50E-03 | 1.40E-02 | |
| Steroid hydroxylase activity | | 7 | 1.80E-03 | 3.80E-02 | |
| Arachidonic acid metabolism | | 10 | 6.10E-03 | 4.00E-02 | |
| Epoxygenase P450 pathway | | 4 | 2.90E-02 | 4.90E-01 | |
| Linoleic acid metabolism | | 6 | 3.90E-02 | 1.80E-01 | |
| Inflammatory mediator regulation of TRP channels | | 7 | 3.40E-01 | 7.60E-01 | |
| Serotonergic synapse | | 4 | 8.80E-01 | 9.90E-01 | |
| Annotation Cluster 11: Enrichment Score: 5.95 | | NAD | 24 | 1.30E-12 | 2.40E-11 |
| | | Nucleotide phosphate-binding region: NAD | 13 | 6.20E-04 | 4.00E-02 |
| | | Binding site: NAD | 11 | 1.70E-03 | 8.90E-02 |
| Annotation Cluster 12: Enrichment Score: 5.8 | | Lipid metabolism | 23 | 5.60E-13 | 1.10E-11 |
| | Serine esterase | 10 | 1.60E-08 | 1.90E-07 | |
| | Carboxylic ester hydrolase activity | 14 | 6.60E-08 | 3.40E-06 | |
| | Carboxylesterase type B, active site | 8 | 2.30E-07 | 2.30E-05 | |
| | Carboxylesterase type B, conserved site | 8 | 1.10E-06 | 8.50E-05 | |
| | Carboxylesterase, type B | 8 | 1.40E-06 | 1.00E-04 | |
| | Drug metabolism - other enzymes | 8 | 2.80E-03 | 2.10E-02 | |
| | Active site: Acyl-ester intermediate | 4 | 4.50E-03 | 1.80E-01 | |
| | Active site: Charge relay system | 11 | 2.10E-02 | 5.20E-01 | |

Supplementary Table 9.Continued

| Annotation of the functional clustering | | n | P value | Benjamini |
|---|---|----|----------|-----------|
| Annotation Cluster 13: Enrichment Score: 5.47 | Citrate cycle (TCA cycle) | 11 | 1.50E-07 | 3.10E-06 |
| | TCA | 7 | 6.70E-06 | 5.30E-05 |
| | TCA | 7 | 3.80E-05 | 2.80E-03 |
| Annotation Cluster 14: Enrichment Score: 4.97 | Mitochondrion inner membrane | 32 | 3.10E-16 | 9.20E-15 |
| | Electron transport | 14 | 1.60E-07 | 1.70E-06 |
| | Oxidative phosphorylation | 18 | 1.70E-05 | 2.50E-04 |
| | Respiratory chain | 9 | 2.50E-05 | 1.80E-04 |
| | Respiratory chain | 9 | 3.50E-05 | 5.10E-04 |
| | Parkinson's disease | 18 | 4.20E-05 | 4.90E-04 |
| | Mitochondrial respiratory chain complex I | 8 | 6.50E-05 | 9.20E-04 |
| | Huntington's disease | 18 | 1.30E-03 | 1.20E-02 |
| | NAFLD | 15 | 2.30E-03 | 2.10E-02 |
| | Alzheimer's disease | 16 | 2.70E-03 | 2.20E-02 |
| | Ubiquinone | 4 | 1.20E-02 | 5.60E-02 |

ATP, adenosine triphosphate; CoA, coenzyme A; FAD, flavin adenine dinucleotide; NAD, nicotinamide adenine dinucleotide; TCA, tricarboxylic acid cycle; TRP, transient receptor potential.

Supplementary Table 10.Protein Functional Clustering of the Adipose Proteomics

| Annotation of the functional clustering | | n | P value | Benjamini |
|--|------------------------------|---|---------|-----------|
| Annotation cluster 1: Enrichment score: 3.08 | Mitochondrion | 8 | 3.7E-4 | 1.9E-2 |
| | Transit peptide | 6 | 5.0E-4 | 1.8E-2 |
| | Mitochondrial inner membrane | 5 | 2.7E-3 | 8.1E-2 |
| Annotation cluster 2: Enrichment score: 2.14 | Oxidation-reduction process | 8 | 7.5E-5 | 2.2E-2 |
| | Oxidoreductase | 6 | 1.4E-3 | 3.6E-2 |
| | Oxidoreductase activity | 6 | 2.9E-3 | 3.1E-1 |
| | Metabolic pathways | 9 | 1.0E-2 | 4.6E-1 |
| Annotation cluster 3: Enrichment score: 1.06 | Metabolic process | 4 | 3.7E-2 | 9.8E-1 |
| | Lipid metabolism | 3 | 1.0E-1 | 6.2E-1 |
| | Lipid metabolic process | 3 | 1.7E-1 | 1.0E0 |

Supplementary Table 11.Detailed Parameters of the Untargeted Mass Spectrometry Instrument and Liquid Chromatography Gradient

| Q Exactive | Negative |
|-------------------------------------|---|
| Spray voltage, <i>kV</i> | 2.5 ESI- |
| Source temperature, °C | 320 |
| Sheath gas flow rate, <i>Arb</i> | 35 |
| Auxillary gas flow rate, <i>Arb</i> | 10 |
| Mass range, <i>m/z</i> | 80–1200 |
| Full MS resolution | 70,000 |
| MS/MS resolution | 17,500 |
| TopN | 10 |
| Stepped NCE | 30 |
| Duty cycle (s) | ~1.2 |
| LC condition | |
| Column, <i>mm</i> , BEH | 2.1 × 100 |
| Column chamber T, °C | 40 |
| Flow rate, <i>mL/min</i> | 0.25 |
| Mobile phase A | 10 mM NH ₄ Ac 95% ACN 5% H ₂ O |
| Mobile phase B | 10 mM NH ₄ Ac 50% ACN 50% H ₂ O |
| Gradient, A % | |
| 2 min | 95 |
| 4 min | 80 |
| 6 min | 68 |
| 8 min | 55 |
| 11 min | 48 |
| 14 min | 42 |
| 16 min | 34 |
| 18 min | 15 |
| 19 min | 5 |
| 21 min | 5 |
| 21.1 min | 95 |
| 25 min | 95 |

NCE, normalized collision energy.

Supplementary Table 12.Metabolites Multiple Reaction Monitoring List for Targeted Liquid Chromatography–Mass Spectrometry Detection

| Metabolites | Q1 mass, <i>Da</i> | Q3 mass, <i>Da</i> |
|-------------|--------------------|--------------------|
| Cer 16:0 | 538.2 | 264.2 |
| Cer 18:0 | 566.2 | 264.2 |
| Cer 18:1 | 564.2 | 264.2 |
| Cer 20:0 | 594.2 | 264.2 |
| Cer 22:0 | 522.2 | 264.1 |
| Cer 24:0 | 650.7 | 264.2 |
| Cer 24:1 | 648.4 | 264.4 |
| Cer 19:0 | 580.2 | 264.2 |
| Cer 19:0 | 580.2 | 562.3 |
| FFA 18:2 | 325.2 | 325.2 |
| FFA 19:0 | 297.3 | 297.3 |
| FFA 12:0 | 199.2 | 199.2 |
| FFA 20:0 | 311.3 | 311.3 |
| FFA 22:0 | 339.3 | 339.3 |
| FFA 20:5 | 301.2 | 301.2 |
| FFA 20:2 | 307.3 | 307.3 |
| FFA 20:4 | 349.2 | 349.2 |
| FFA 22:6 | 327.2 | 327.2 |
| FFA 20:1 | 309.3 | 309.3 |
| FFA 16:0 | 301.2 | 255.2 |
| FFA 16:1 | 327.3 | 281.2 |
| FFA 14:0 | 273.2 | 227.2 |
| FFA 18:0 | 329.3 | 283.3 |
| C16 | 400.2 | 84.7 |
| C0 | 162.1 | 85 |
| C8 | 268.1 | 85 |
| C10 | 316.2 | 85 |
| C12 | 344.3 | 85 |
| C14 | 372.1 | 85 |
| C6 | 260.2 | 84.7 |
| C3 | 218.2 | 84.8 |
| C2 | 204.1 | 85 |
| C4 | 232.1 | 84.8 |
| C6 | 246.1 | 84.8 |

Supplementary Table 13.List of Primers Used and Their Sequences

| Gene | | Primer Sequences |
|---------|---------|--------------------------|
| 18S | Forward | GTAACCCGTTGAACCCATT |
| | Reverse | CCATCCAATCGGTAGTAGCG |
| CD36 | Forward | GGCAGGAGTGCTGGATTA |
| | Reverse | GAGGCGGGCATAAGTATCA |
| LPL | Forward | ACTAGGTCCCACAGGACTG |
| | Reverse | GACTTCCAGAAGTAACCAACTTTG |
| MTP | Forward | GGAAAGCAGAGCGGAGAC |
| | Reverse | AGAGCAAGGGTCAGGCAC |
| Acadl | Forward | TCTTTTCTCGGAGCATGACA |
| | Reverse | GACCTCTCTACTCACTTCTCCAG |
| Acadvl | Forward | CTACTGTGCTTCAGGGACAAC |
| | Reverse | CAAAGGACTTCGATTCTGCC |
| Acadm | Forward | AGGGTTTAGTTTTGAGTTGACGG |
| | Reverse | CCCCGCTTTTGTGATATTCCG |
| Scd1 | Forward | TTCTTGCGATACACTCTGGTGC |
| | Reverse | CGGGATTGAATGTTCTTGTGCGT |
| M-Fasn | Forward | TTGCTGGCACTACAGAATGC |
| | Reverse | AACAGCCTCAGAGCGACAAT |
| Cpt1b | Forward | AAGAGACCCCGTAGCCATCAT |
| | Reverse | GACCCAAAACAGTATCCAATCA |
| CPT2 | Forward | GAAGAAGCTGAGCCCTGATG |
| | Reverse | GCCATGGTATTTGGAGCACT |
| CPT1a | Forward | AACCCAGTGCCCTAACGATG |
| | Reverse | GAACTGGTGGCCAATGAGAT |
| ACC1 | Forward | ATTGGGCACCCCAGAGCTA |
| | Reverse | CCCGCTCCTTCAACTTGCT |
| M-Bbox1 | Forward | AGAGTCCCTCTACCCAGCAG |
| | Reverse | TGGTCATTGGGCCATGTGAT |
| HSL | Forward | CCAGCCTGAGGGCTTACTG |
| | Reverse | CTCCATTGACTGTGACATCTCG |
| ATGL | Forward | GGATGGCGGCATTTTCAGACA |
| | Reverse | CAAAGGGTTGGGTTGGTTCAG |